CHAPTER IV

RESULTS AND DISCUSSION

4.1 Co-Cultivation: Adaptive Laboratory Evolution

Using adaptive laboratory evolution protocol, *Streptomyces* sp. SSUT88A competed against three different pathogens. The approximately 220-day-long competition experiments yielded 4 adapted strains after the ninth (IX) cycle of adaptation-selection based on their highest antimicrobial activities across the same co-culturing condition. The strains were designated as SSUT88A$^{Ab9\text{-}5}$ (SSUT88A co-cultured with *Acinetobacter baumannii* SUTH-Isolate), SSUT88A$^{MR9\text{-}16}$ (SSUT88A co-cultured with MRSA20651), SSUT88A$^{N90PS9\text{-}32}$ (SSUT88A co-cultured with *Pseudomonas aeruginosa* SUTH-Isolate N90PS), and SSUT88A$^{3P9\text{-}1}$ (SSUT88A co-cultured with all 3 pathogens mentioned above). The adapted strains exhibited no visually different morphological character from their parental strain (Figure 4.1).

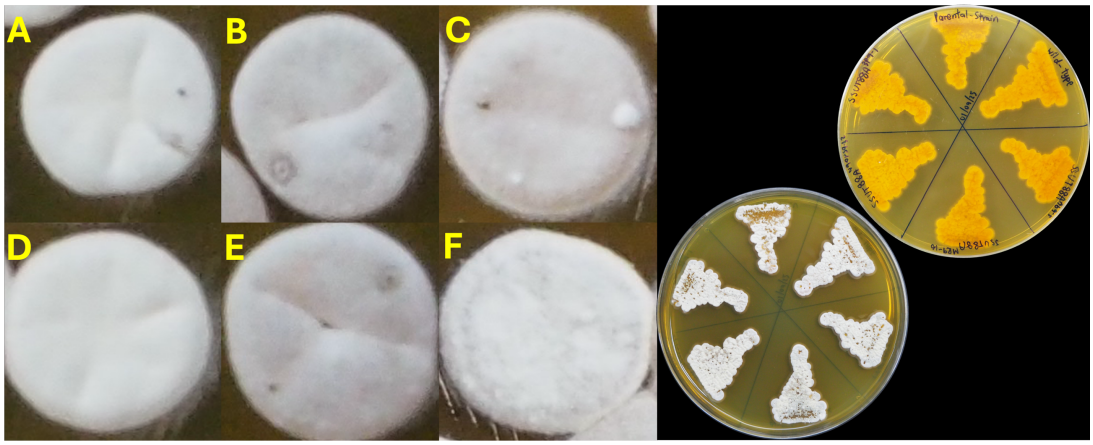

Figure 4.1 Colony morphology of *Streptomyces* sp. SSUT88A parental strain (A) and its adapted strains SSUT88A^{WT} (B), SSUT88A$^{Ab9\text{-}5}$ (C), SSUT88A$^{MR9\text{-}16}$ (D), SSUT88A$^{N90PS9\text{-}32}$ (E), SSUT88A$^{3P9\text{-}1}$ (F) grown on ISP-2 medium at 30 °C for 7 Days.

4.2 Crude Extraction of Bioactive Compounds

The cell-free supernatant after adaptation was extracted twice with ethyl acetate (1:1 v/v) by vigorously shaking in the separatory funnel and left to allow phase separation at room temperature. The ethyl acetate layer containing crude compound was evaporated to dryness. The dried crude extract was weighed to assess each strain's ability to produce crude extract. After nine cycles of adaptation, MRSA was the most potent pathogen to trigger the production of crude compound, with a 46.3% increase compared to the average wild-type (WT) crude compound production. This was followed by *A. baumannii* which induced 32.6% increase. Quadri-culture co-cultivation (3-pathogens combination) showed a lower triggering effect, increasing the crude compound production by only 5.1%, while *P. aeruginosa* led to a reduce crude compound production by 5.1% compared to the WT average. Statistical analysis was performed using one-way ANOVA followed by Tukey's HSD multiple comparison test (p-value < 0.05). Among these, only crude extract produced from MRSA and *A. baumannii* were statistically significant difference at (Figure 4.2).

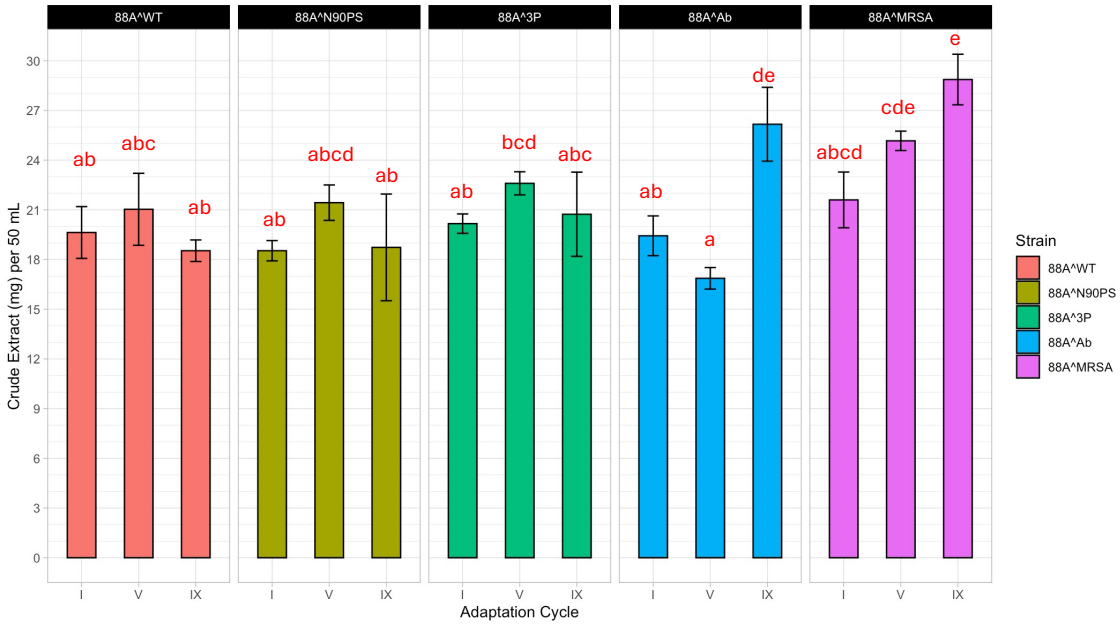

Figure 4.2 Quantity of crude extracts (mg) from each strain through adaptation cycles (n=3). 88A^WT: SSUT88A^{WT}; 88A^Ab: SSUT88A$^{Ab9\text{-}5}$; 88A^MRSA: SSUT88A$^{MR9\text{-}16}$; 88A^N90PS: SSUT88A$^{N90PS9\text{-}32}$; 88A^3P: SSUT88A$^{3P9\text{-}1}$.

The ratio of crude extract to total cell dry weight (mg/g) was used to calculate the yield, offering insight into how efficiently each strain produces its crude bioactive compounds. In the case of wild-type, a gradual decline in yield was observed along adaptation cycles, suggesting that prolonged subculturing may shift its metabolic priorities away from secondary metabolite production. For SSUT88A$^{N90PS9-32}$ and SSUT88A^{3P9-1}, yield fluctuated over the course of the adaptation without a consistent upward or downward trend, implying that co-cultivation with these pathogens may not strongly promote or suppress metabolite production but instead cause varying metabolic responses across cycles. SSUT88A^{Ab9-5} exhibited the highest overall yield, showing a 43% increase compared to the wild-type average followed by SSUT88A^{MR9-16} with a 40% increase. However, statistical analysis using one-way ANOVA followed by Tukey's HSD post hoc test showed no significant difference between these two groups ($p > 0.05$). In contrast, SSUT88A^{3P9-1} showed only a 4% increase, while SSUT88A$^{N90PS9-32}$ had a 7% decrease in yield compared to the wild-type. These differences were also not statistically significant.

The substantial increase in crude extract production observed in strain SSUT88A^{MR9-16}, co-cultured with MRSA, may be attributed to the wild-type *Streptomyces* sp. SSUT88A's prior antimicrobial activity against this pathogen. Although weaker, a similar effect was also observed against *A. baumannii*, which may partly explain the enhanced production in SSUT88A^{Ab9-5}. The presence of these pathogens likely imposed a comparatively moderate selective pressure during co-cultivation, potentially providing favorable conditions for adaptive shifts in secondary metabolism. Furthermore, the two positively adapted strains, demonstrated different crude compound production elevation profile. SSUT88A^{MR9-16} gradually and steadily increase from cycle-1 until cycle-9, while SSUT88A^{Ab9-5} seems to decrease at the earlier cycle (CI-IV) but strike back at the ninth adaptation cycle, these differences may reflect distinct adaptive strategies, where stable enhancement in biosynthetic output requires varying durations of exposure depending on the selective environment.

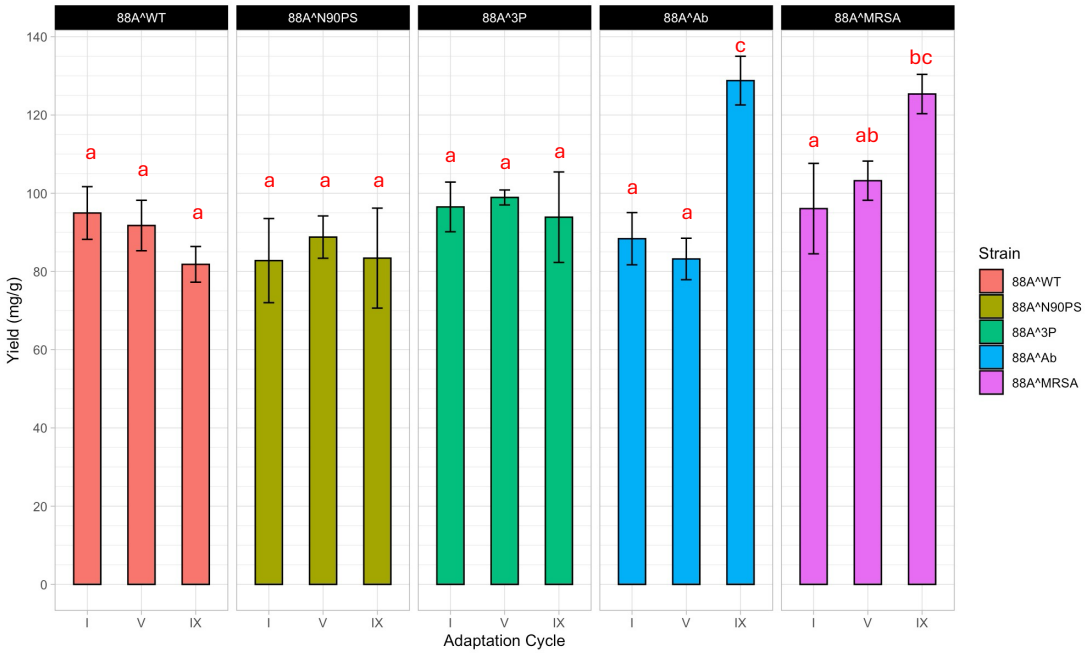

Figure 4.3 Yield of crude extracts from each strain through adaptation cycles (crude extract weight (mg)/ cell dry weight (g)). All experiments were conducted in triplicate. 88A^WT: SSUT88A^{WT}; 88A^Ab: SSUT88A$^{Ab9\text{-}5}$; 88A^MRSA: SSUT88A$^{MR9\text{-}16}$; 88A^N90PS: SSUT88A$^{N90PS9\text{-}32}$; 88A^3P: SSUT88A$^{3P9\text{-}1}$.

4.3 Antimicrobial Activity Assessment

To evaluate the bioactive potential of the adapted *Streptomyces* strains, a set of antimicrobial assays were performed to provide a comprehensive aspect of how co-cultivation influences the spectrum, strength, and timing of antimicrobial compound production in response to different selective pressures.

4.3.1 Primary Antimicrobial Activity: Agar Well Diffusion

Throughout the adaptation process, agar well diffusion assays revealed that the antimicrobial activity of crude compound produced by each strain as shown in Figure 4.4. The wild-type strain's antimicrobial activities remained relatively stable, with only minor fluctuations in inhibition zones against both Gram-positive and Gram-negative pathogens, suggesting that, in the absence of selective pressure no spontaneous upregulation or suppression was observed across cycles, the strain maintains a consistent level of bioactive compound production. Evidently, notable enhancements in antimicrobial activity were observed in strains adapted through co-

cultivation with specific suitable pathogens. Particularly, SSUT88A$^{MR9\text{-}16}$ and SSUT88A$^{Ab9\text{-}5}$ displayed significantly increased inhibition zones by cycle 9, most obvious against Gram-positive bacteria, MRSA and methicillin-resistant *Staphylococcus epidermidis* (MRSE). A moderate increase in inhibition was also noticed against Gram-negative bacteria (e.g., *A. baumannii,* MDR-*E. coli* and MDR-*P. aeruginosa*), even though the enhancement was less pronounced, the relative increase is rather similar.

On the other hand, strains SSUT88A$^{N90PS9\text{-}32}$ and SSUT88A$^{3P9\text{-}1}$ did not exhibit consistent improvements in antimicrobial activity, demonstrating variable with some slightly reduced inhibition profiles over time, implying that the respective co-cultivation conditions may not have provided a suitable selective pressures for the enhancement of bioactive compound production. Antimicrobial activity against *Klebsiella pneumoniae* 1617 SUTH-isolate was not observed in any strain, thus is not reported in this work.

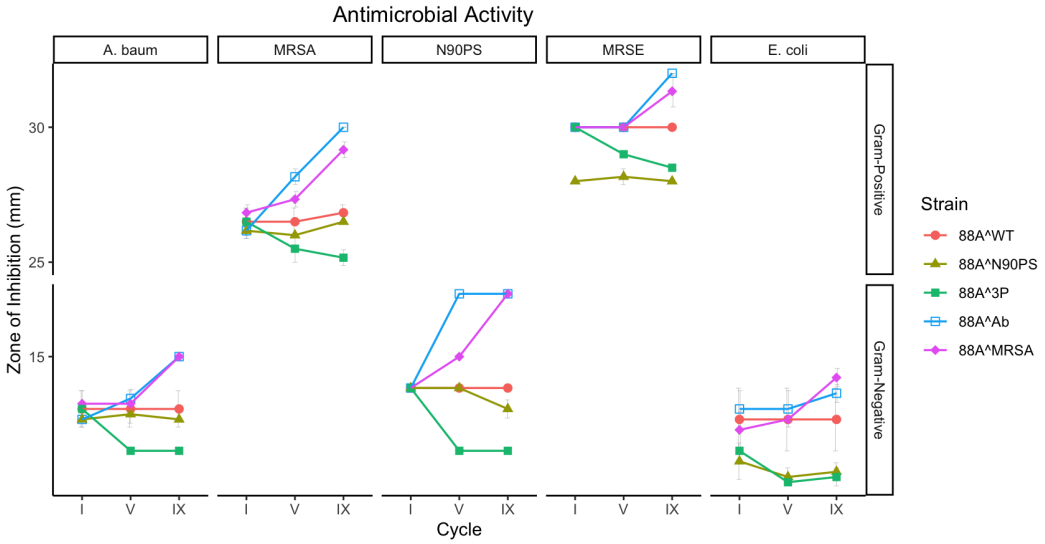

Figure 4.4 Antimicrobial activities of crude extracts from each strain across adaptation cycles 1, 5, and 9 (n=3). The pathogens are divided into Gram-positive and Gram-negative which use different Y-axis scale. Strains are denoted on the right legend, 88A^WT: SSUT88A^{WT}; 88A^Ab: SSUT88A$^{Ab9\text{-}5}$; 88A^MRSA: SSUT88A$^{MR9\text{-}16}$; 88A^N90PS: SSUT88A$^{N90PS9\text{-}32}$; 88A^3P: SSUT88A$^{3P9\text{-}1}$.

4.3.2 Time-Course Antimicrobial Activity

Throughout the adaptation process, one strain exhibiting complete loss of antimicrobial activity was isolated from the co-culture with the three-pathogen combination at the sixth adaptation cycle. This strain was designated as SSUT88A^{3P6-7} and was included as a negative adaptation effect in subsequent analyses. The strains, SSUT88A$^{N90PS9-32}$ and SSUT88A^{3P9-1}, which showed minimal difference in crude extract production, yield, and primary antimicrobial activity throughout the adaptation process, were excluded from further investigation.

Morphological observations revealed that while the wild-type strain and positively adapted strains (SSUT88A^{MR9-16} and SSUT88A^{Ab9-5}) exhibited similar colony appearance which characterized by dark orangish-yellow pigmentation and diffusible pigment, the SSUT88A^{3P6-7} strain exhibited notable morphological alterations. The characteristic yellow diffusible pigment, likely associated with antimicrobial compound production, was absent and the colony pigmentation shifted toward a more reddish hue. These morphological differences support the observed loss of bioactivity and suggest metabolic or regulatory alterations. (Figure 4.5)

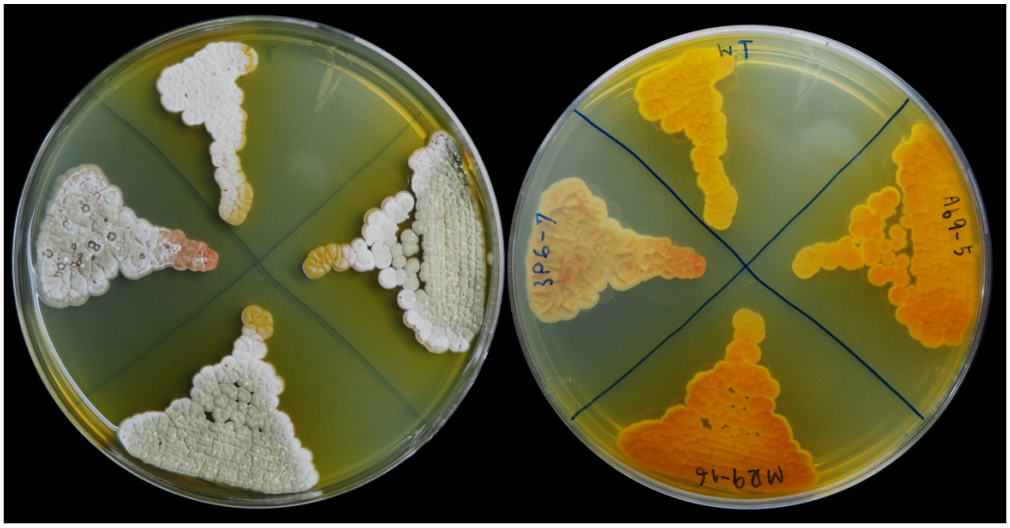

Figure 4.5 Colony appearances of wild-type SSUT88A, SSUT88A^{MR9-16}, SSUT88A^{Ab9-5}, and SSUT88A^{3P6-7} (strain with activity loss).

Using MRSA DMST20651, which possess high susceptibility to bioactive compound produced from SSUT88A, as a representative pathogen for the most

sensitive model, a time-course antimicrobial assessment was conducted (Figure 4.6). Among tested isolates, SSUT88A^{Ab9-5} exhibited the earliest onset of detectable antimicrobial activity, beginning on day 2 and reaching the highest inhibition around days 5–6, while sustained the activity across experimentation period. In contrast, SSUT88A^{MR9-16} and the wild-type strain displayed similar production profiles, with inhibition zones appearing around days 3–4 and reaching maximal activity by approximately day 10. Moreover, SSUT88A^{3P6-7} failed to exhibit any observable antimicrobial activity over the entire 14-day incubation period, confirming that its loss of bioactivity is not from the compound stability over time.

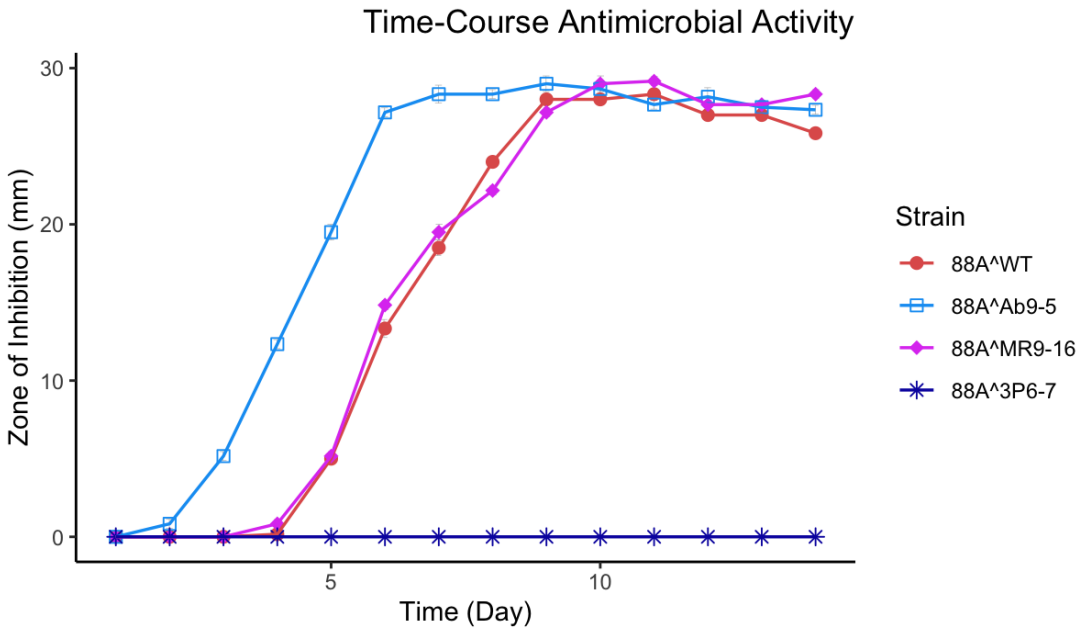

Figure 4.6 Antimicrobial activities monitoring by observing antimicrobial compound production of each strain over the course of 14 days (n=3). MRSA DMST20651 was used as the representative tested pathogens.

4.3.3 Secondary Antimicrobial Activity: MIC and MBC

MIC and MBC assays were conducted to evaluate the potency of crude extracts from selected strains against 6 drug-resistant pathogens in terms of secondary antimicrobial activity (Table 4.1). The wild-type strain displayed moderate antimicrobial activity, particularly against Gram-positive bacteria, MRSA and MRSE, with MICs of 2 µg/mL. In contrast, co-cultivation with MRSA or *A. baumannii* greatly enhanced the

antimicrobial activity of the adapted strains (SSUT88A^{MR9-16} and SSUT88A^{Ab9-5}). Both strains exhibited 4–8-fold lower MIC values against MRSA and MRSE (0.25–0.5 µg/mL) compared to the wild-type, as well as decreased MBC values (32 µg/mL), indicating stronger inhibition and bactericidal effects. Additionally, these strains also showed improvements in MIC and MBC values against *A. baumannii* and *E. coli*. On the other hand, very limited differences were observed in MIC values against *K. pneumoniae* and in MBC values against *P. aeruginosa*, while no differences were observed in MBC against *K. pneumoniae* or MIC against *P. aeruginosa* across all strains. Regardless, all strains required very high concentrations of crude extract to inhibit or kill these pathogens. On the other hand, SSUT88A^{3P6-7}, adapted through co-culture with all three pathogens, completely lost measurable antimicrobial activity across all tested organisms (MIC and MBC >2,048 µg/mL), aligning with earlier time-course and inhibition zone findings.

Table 4.1 Minimum inhibitory concentration (MIC) and minimum bactericidal concentration (MBC) values (µg/mL) of crude extracts from selected *Streptomyces* sp. SSUT88A strains. All experiments were conducted in triplicate.

Drug-Resistant Pathogen	2nd Antimicrobial Activity (MIC/MBC in µg/mL)			
	Wild-type	SSUT88A^{MR9-16}	SSUT88A^{Ab9-5}	SSUT88A^{3P6-7}
MRSA	2/64	0.25/32	0.5/32	>2,048/>2,048
A. baumannii	1,024/1,024	512/512	512/512	>2,048/>2,048
P. aeruginosa	1,024/>2,048	1,024/2,048	1,024/>2,048	>2,048/>2,048
MRSE	2/64	0.25/32	0.5/32	>2,048/>2,048
E. coli	2,048/2,048	1,024/1,024	1,024/1,024	>2,048/>2,048
K. pneumoniae	2,048/>2,048	1,024/>2,048	1,024/>2,048	>2,048/>2,048

Pathogens Used: MRSA – DMST20651; *A. baumannii* – MDR, SUTH-Isolate; *P. aeruginosa* – N90PS, MDR, SUTH-Isolate; MRSE – methicillin-resistant, SUTH-Isolate; *E. coli* – 2026, MDR, SUTH-Isolate; *K. pneumoniae* – 1617, MDR, SUTH-Isolate.

These results demonstrate the potential of adaptive laboratory evolution using co-cultivation to enhance antimicrobial compounds that were already present in the wild-type strain, either by accelerating their production, as seen in the

precocious activity of SSUT88A^{Ab9-5}, or by increasing their potency, as demonstrated by SSUT88A^{MR9-16}. This enhancement could help reduce antibiotics production costs by shortening fermentation time and improving yield efficiency. Moreover, these findings reflect the dynamic nature of microbial adaptation under ecological pressure, which can be strategically harnessed to fine-tune secondary metabolite expression. Further studies to isolate and characterize the upregulated compounds may shed light on their mechanisms of action and reveal novel paths for antimicrobial development.

4.4 Whole Genome Sequencing, Assembly, and Visualization

4.4.1 Genomic DNA Extraction, Sequencing, and Quality Control

Among all adapted strains, three representative strains were selected for whole genome sequencing and comparative analysis, including SSUT88A^{Ab9-5} and SSUT88A^{MR9-16}, which showed most prominent enhancement in antimicrobial activity after adaptive co-culture, and SSUT88A^{3P6-7}, a strain isolated from the cycle-VI of adaptation with a three-pathogen combination that exhibited a complete loss of bioactivity. The genomic DNA was successfully extracted from all strains, and subsequent Illumina sequencing yielded high-quality paired-end reads. The raw reads were processed using fastp v0.23.4, which conducted adapter trimming, quality filtering, and per-read quality control. Final Q30 scores >96% and average GC content around 69-71%, consistent with Streptomyces high GC content description (Ramasamy and Sudalaimuthu, 2022).

4.4.2 Genome Assembly and Assessment

Unicycler v0.5.0 with the conservative mode was used to assemble the high-quality reads into draft genomic sequences. The resulting assemblies were evaluated using QUAST and CheckM to determine structural metrics and completeness. All assembled genomes exhibited characteristics consistent with typical *Streptomyces* species, with large genome sizes ranging from 10.2 to 11.1 Mbp and GC content averaging around 72% relating to fastP data before assembly. The number of contigs varied strains (241–548). CheckM analysis, detected Streptomycetaceae family accurately and used as marker, further confirmed high assembly completeness, with all strains showing >99% completeness and <2% contamination.

The genome assembly of the wild-type strain was approximately 1 Mbp larger than that of the adapted strains. This difference is likely caused by the higher sequencing depth and different sequencing provider used for the wild-type, potentially capturing more low-abundance or repetitive regions. Despite this variation, the assembly quality (e.g., N50, completeness) was high across all samples (Table 4.2), supporting the use of the wild-type genome as a suitable reference for downstream comparative analyses. Variant analysis and k-mer-based deletion screening were used to further examine the potential for biological significant differences in the adapted strains (Section 3.2.7.4).

Table 4.2 Summary of genome assembly statistics generated by QUAST and CheckM for wild-type and adapted Streptomyces strains. All genomes show high completeness and low contamination, supporting assembly quality.

Variable	**SSUT88A^{WT}**	**SSUT88A^{MR9-16}**	**SSUT88A^{Ab9-5}**	**SSUT88A^{3P6-7}**
Total Length (bp)	11,128,670	10,220,793	10,220,825	10,310,976
GC-Content (%)	71.55	71.66	71.66	71.69
Contigs	548	242	248	241
Largest Contigs	186,269	345,593	427,242	375,625
N50	46,449	112,456	102,227	112,652
N90	11,786	26,695	26,277	28,351
L50	80	26	28	26
L90	287	92	99	92
Completeness* (%)	99.94	99.94	99.94	99.94
Contamination* (%)	1.29	1.07	1.07	1.07

* Genome completeness and contamination is assessed by CheckM v1.2.2

4.4.3 Genome Annotation and Visualization

Genome annotation using Prokka predicted 9,530; 9,011; 9,008; and 8,965 coding sequences for SSUT88A^{WT}; SSUT88A^{MR9-16}; SSUT88A^{Ab9-5}; and SSUT88A^{3P6-7}, genome respectively. The number and types of annotated features were

largely consistent across wild-type and adapted strains, showing the overall genomic conservation.

Circular genome maps generated by Proksee provided an overview of the genomic architecture. The illustrated features are locations of CDSs, tRNAs, tmRNAs, GC-content and GC-skewness. The annotated regions were distributed throughout the chromosomes (Figure 4.7, A-D). Detailed comparative analyses of genome structure and feature distribution, including mobile genetic elements and putative transferred regions, are further discussed in Section 3.2.7.4.

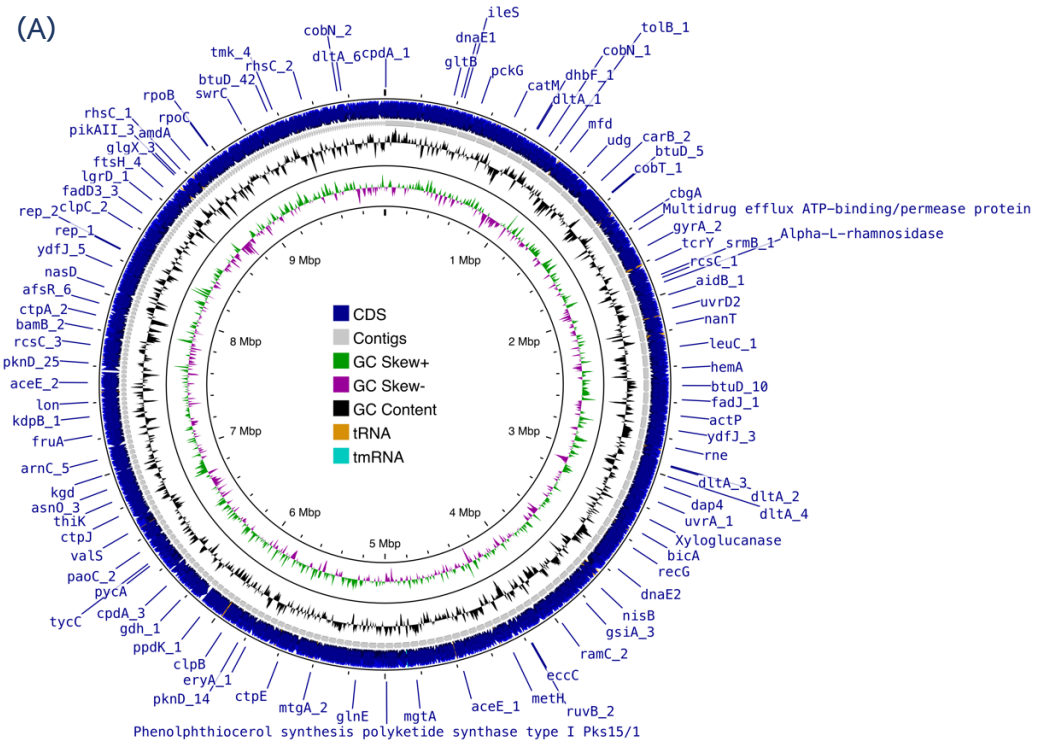

Figure 4.7 Draft genome maps of *Streptomyces* sp. SSUT88A strains generated by Proksee. CDSs are marked in dark blue, Contigs are represented in grey arrows. The green and purple illustrate GC skew+ and GC skew-, respectively, and the black represent GC content. (A) SSUT88A^{WT}; (B) SSUT88A$^{MR9\text{-}16}$; (C) SSUT88A$^{Ab9\text{-}5}$; and (D) SSUT88A$^{3P6\text{-}7}$.

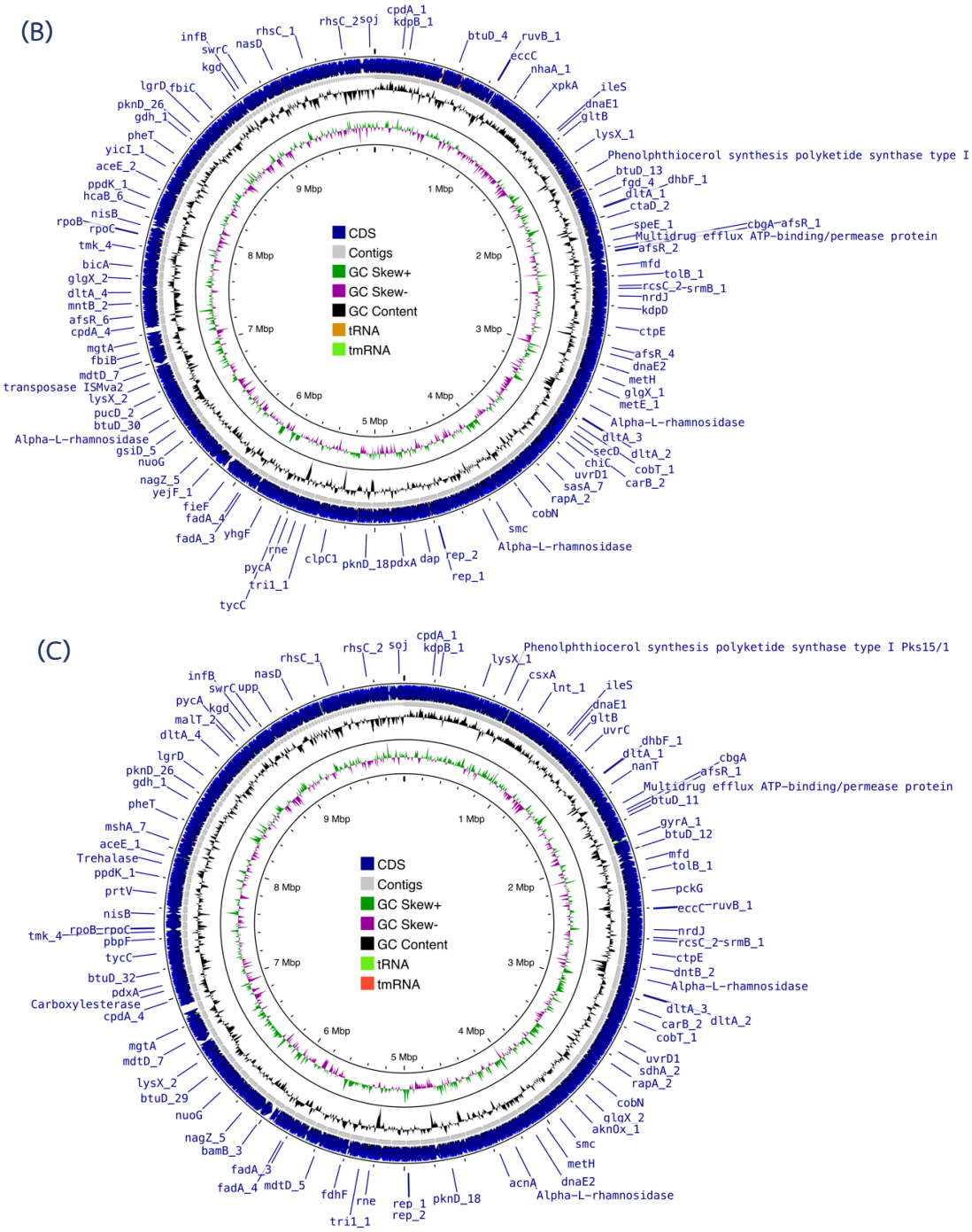

Figure 4.7 (Continued) Draft genome maps of *Streptomyces* sp. SSUT88A strains generated by Proksee. CDSs are marked in dark blue, Contigs are represented in grey arrows. The green and purple illustrate GC skew+ and GC skew-, respectively, and the black represent GC content. (A) SSUT88A^{WT}; (B) SSUT88A$^{MR9\text{-}16}$; (C) SSUT88A$^{Ab9\text{-}5}$; and (D) SSUT88A$^{3P6\text{-}7}$.

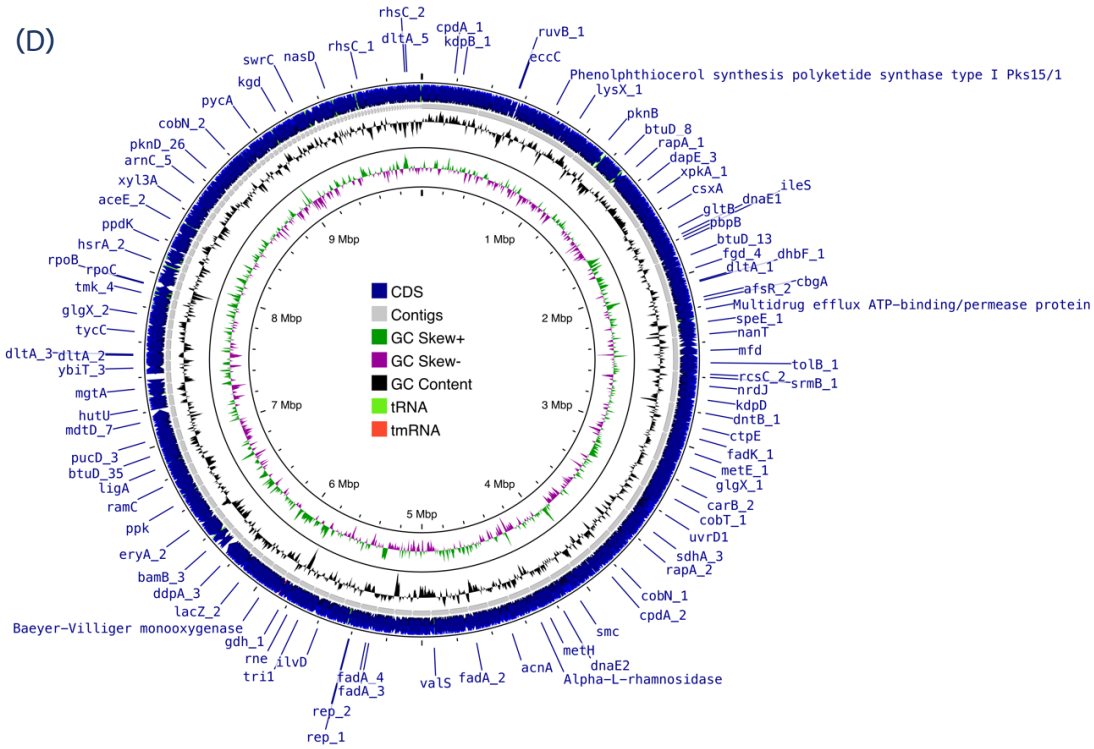

Figure 4.7 (Continued) Draft genome maps of *Streptomyces* sp. SSUT88A strains generated by Proksee. CDSs are marked in dark blue, Contigs are represented in grey arrows. The green and purple illustrate GC skew+ and GC skew-, respectively, and the black represent GC content. (A) SSUT88A^{WT}; (B) SSUT88A$^{MR9\text{-}16}$; (C) SSUT88A$^{Ab9\text{-}5}$; and (D) SSUT88A$^{3P6\text{-}7}$.

4.5 Functional and Comparative Genomic Analysis

4.5.1 Taxonomic Comparisons

Comparative taxonomic analyses confirmed that the wild-type and the adapted strains belong to the same species, therefore excluding the possibility of any contamination during the adaptation or sequencing processes. dDDH values exceeded 99.5%, and ANI values calculated based on both Blast+ (ANIb) and MUMmer (ANIm) were consistently above 99.5%, well above the commonly accepted species-level thresholds. Pairwise Tetra-Correlation analysis also supported species identity, with all pairwise comparisons correlation coefficients above 0.999 cut-off. Moreover, Phylogenomic tree based on whole-genome sequences showed tight clustering of all strains (Figure 4.8).

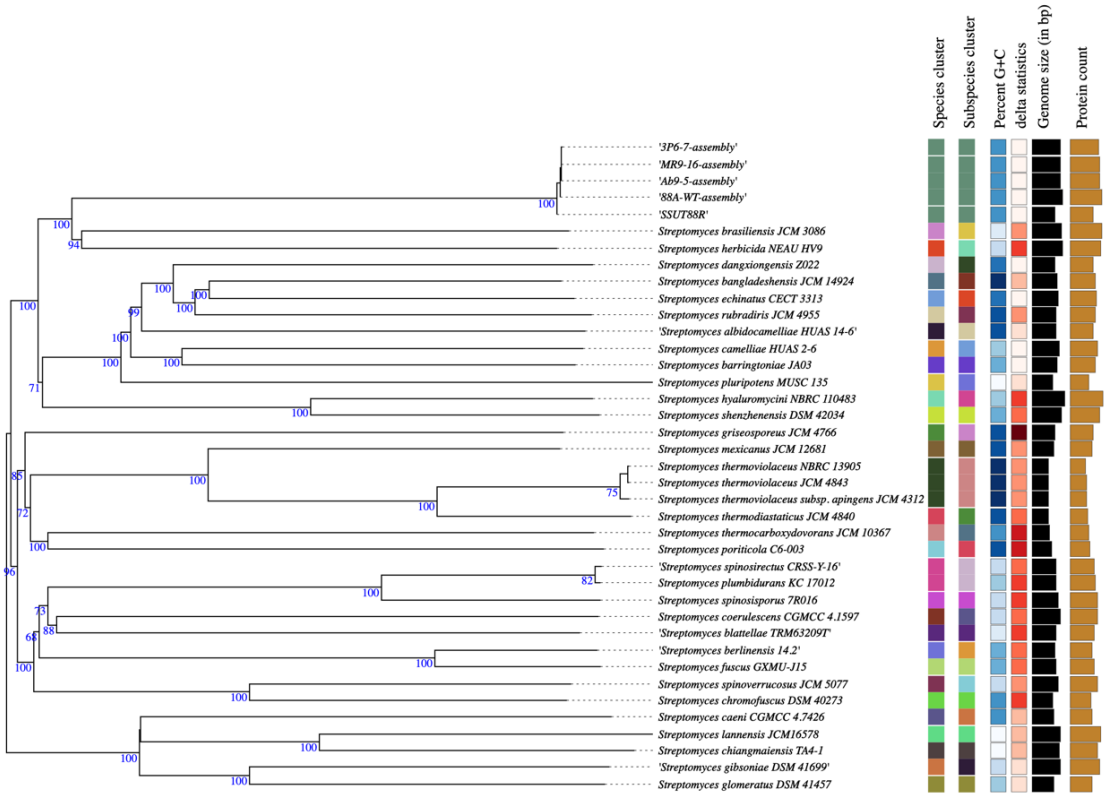

Figure 4.8 Phylogenomic tree of wild-type and evolved *Streptomyces* sp. SSUT88A strains using assembled whole-genome sequence along with their closely related type strain on the TYGS platform.

4.5.2 Antimicrobial Resistance Genes

Based on ResFinder v4.7.2 with default thresholds (>90% identity and minimum length coverage) the wild-type strain does not contain any AMR genes. No acquired AMR genes were detected in any of the evolved strains harbored even after repetitively exposed to drug-resistant pathogens.

4.5.3 Secondary Metabolite Biosynthetic Gene Clusters

Presence/absence analysis of BGCs, predicted by antiSMASH, revealed variation between the wild-type and evolved strains. While several BGCs in the wild-type retain in all evolved strains, others were found exclusively in antibiotics producing strains (wild-type, SSUT88A$^{MR9\text{-}16}$ and SSUT88A$^{Ab9\text{-}5}$), one or more of the high-producing strains (SSUT88A$^{MR9\text{-}16}$ and SSUT88A$^{Ab9\text{-}5}$) or uniquely retained in the wild-type and non-producer (SSUT88A$^{3P6\text{-}7}$). All conserved clusters across all strains are summarized in

Appendix A for reference. The strain-specific and differentially distributed clusters focusing on potential biological relevance are presented in Table 4.3.

The antibiotic producer strains (wild-type, SSUT88A^{MR9-16} and SSUT88A^{Ab9-5}) shared six clusters which are absent in the non-producing SSUT88A^{3P6-7}, suggesting the contribution to core secondary metabolism linked to antibiotic activity. By product type, the clusters found are predicted to synthesize:

- Lanthipeptide-Class-III / NAPAA Hybrid Cluster: A shared cluster among wild-type, SSUT88A^{MR9-16} and SSUT88A^{Ab9-}shows biosynthetic features consistent with both lanthipeptide-class-III and Non-alpha poly-amino acids like e-Polylysin (NAPAA) core biosynthetic genes. This prediction suggests the cluster may encode for either or both compound types.
- Terpene: one terpene BGCs (~21,607 bp) was found, this cluster does not correspond to known terpene pathways, hopene or geosmin, which were present in all four strains, suggesting it may encode an uncharacterized compound. Since terpenoid compounds and their derivatives are extremely diverse and have been demonstrated to have antimicrobial, antifungal, anti-inflammatory, antiviral, immunomodulatory, antioxidant or antitumor activities (Duttaroy, 2021), this BGC exclusive presence in the antibiotic-producing group may take functional role in antimicrobial activity, though further experiment would be needed to determine its product and its activity.
- Nucleoside: A nitrogen-containing heterocyclic nitrogenous base and a pentose sugar (Huang et al., 2014), even though mostly related to fundamental building block of DNA and RNA, nucleosides and their derivatives are found to exhibit wide biological activities including antimicrobial (Zhang et al., 2022), with no exceptions to most categories of antibiotics, nucleoside antibiotics are also found to be produced by *Streptomyces* sp. In this analysis, nucleoside BGC was exclusively found in the antibiotic-producers. Although no known compound could be confidently assigned to this cluster, its conserved presence in the active

strains implies a possible association with the antibiotic-producing phenotype.

- Benzoxazole (Most similar know cluster showed Mycemycin C/A/B with medium confidence): Mycemycins are benzoxazole antibiotics, more specifically dibenzoxazepinone group, known for weak a HIV-1 reverse transcriptase inhibitory effect (Liu et al., 2015). While the similarity confidence failed to certainly confirm mycemycin clusters, the prediction suggests the potential for production of closely related molecules. The fact that they were only detected in antibiotic-producing strain strengthen the possible involvement in the observed antimicrobial activity.
- Aryl polyenes: known to be membrane-associated yellow pigments produced by various bacteria (Schöner et al., 2016). They are structurally similar to carotenoids and functionally act as antioxidants, protecting cells from oxidative stress caused by reactive oxygen species (ROS). Present in these strains with antimicrobial activity and visually yellow colored, this BGC may contribute or at least take part in their antibiotics production, yellow pigmentation and increased fitness. Although further experimental validation would be required to confirm this role, some compound like spinamycin has been demonstrated to have antifungal activities and produced from *Streptomyces* (Kawai et al., 2023).

The positively adapted strains defined by increased antimicrobial activity (SSUT88A$^{MR9\text{-}16}$ and SSUT88A$^{Ab9\text{-}5}$) shared two types of clusters which are NRPS and Type I Polyketide Synthase (T1PKS).

Two NRPS clusters were uniquely shared between them, one of these clusters was annotated with low-confidence similarity to actinomycin D, spanning part of one core biosynthetic genes and some additional genes. Actinomycin D is a well-characterized antibiotic produced by *Streptomyces* sp. and is known for its antimicrobial against Gram-positive bacteria (Xia et al., 2022; Zimowska et al., 2024).

Although the annotation confidence was low, the presence of this cluster exclusively in the two strains exhibiting enhanced antimicrobial activity suggests it may contribute to this phenomenon.

In addition, one T1PKS cluster was also identified exclusively between them. T1PKSs are large modular enzymes responsible for the synthesis of various polyketide antibiotics in *Streptomyces* (Wang et al., 2020). Although no strong match to known compounds was found for this cluster, its presence only in the enhanced bioactivity strains makes it a candidate of interest. It is possible that this cluster encodes a novel or modified polyketide compound with antimicrobial activity, potentially contributing to the elevated activity observed in these strains.

Although the annotation confidence was low, the exclusive presence of this cluster in the two strains with enhanced antimicrobial activity opens the possibility that it encodes a novel or modified compound contributing to the observed phenotype.

Lastly, a group of BGCs was identified as being present only in the wild-type and the non-producing SSUT88A^{3P6-7} strain, but absent in antibiotic-enhanced strains. These include a lanthipeptide-class-III, redox-cofactor, T1PKS cluster predicted to produce butyrolactol A, a type III polyketide synthase (T3PKS) cluster associated with germicidin biosynthesis, and an aminopolycarboxylic acid cluster linked to ethylenediaminesuccinic acid hydroxyarginine (EDHA) production.

Lanthipeptides are often associated with morphogenetic (Kodani et al., 2005; Takano et al., 2017; Wang and van der Donk, 2012) and antimicrobial activity (Völler et al., 2012). The redox-cofactor component may play a supportive metabolic role and some was proposed to be essential for antimicrobial production (Wang et al., 2013). Butyrolactol A is primarily reported as an antifungal compound, while it demonstrates potent antifungal activity, it's antibacterial aspects remain unclear (Chen et al., 2025). Germicidin is involved in auto-inhibition of spore germination in *Streptomyces*, helping regulate the initiation of growth under unfavorable conditions (Aoki et al., 2011), and the function of EDHA in this context remains unclear. None of these compounds are primarily linked to antibacterial activity, which supports the idea

that these clusters may not be relevant to the enhanced antimicrobial traits observed in other two strains.

Table 4.3 Shared biosynthetic gene clusters presence or absence correlates with each strain. "WT" = wild-type; "3P" = SSUT88A^{3P6-7}; "Ab" = SSUT88A^{Ab9-5}; "MR" = SSUT88AMR$^{9-16}$. The presence of each cluster is indicated with highlighted cell.

Type	Average Size (bp)	Most Similar Known Cluster	Present in Strain			
			WT	MR	Ab	3P
Shared Among Antibiotic-Producers						
Terpene	21,607					
Nucleoside	20,704					
Lanthipeptide-class-iii,NAPAA	42,199					
Benzoxazole	32,650	Mycemycin#				
Arylpolyene	23,960					
Shared Among Increased-Antibiotic-Producing Strains						
NRPS	24,574	Actinomycin D*				
NRPS	8,379					
T1PKS	5,486					
Shared Between wild-type and loss-activity strain						
Lanthipeptide-class-iii	22,567					
Redox-cofactor	21,333					
T1PKS	38,892	Butyrolactol A+				
T3PKS	41,184	Germicide+				
Aminopolycarboxylic-acid	13,457	Ethylenediaminesuccinic acid hydroxyarginine+				

* low, # medium, + high similarity confidence

Overall, the varying patterns of BGC retention and loss across the strains suggest a dynamic genomic response during the adaptation process. One possibility is that genome rearrangements may have contributed to the observed differences in

antimicrobial activity by selectively retaining or eliminating specific biosynthetic clusters. Given the well-known plasticity of *Streptomyces* genomes (Um et al., 2021), particularly in regions associated with secondary metabolism (Bentley et al., 2002), the rearrangements could reflect adaptations favoring more relevant or efficient pathways. However, further experimental validation would be necessary to confirm the functional consequences of these genomic changes.

4.5.4 Orthologous Gene Clustering based on Translated Amino Acid

To investigate differences in functional gene content across strains, orthologous clustering of amino acid sequences annotated by Prokka was performed using OrthoVenn3. A total of 36,812 protein sequences from four *Streptomyces* strains were analyzed, yielding 9,113 orthologous clusters. Of these, 7,714 clusters were conserved across all strains, with 7,230 identified as single-copy orthologs. Only 138 clusters were singletons, representing unique, non-clustered proteins. The clustering also revealed clusters uniquely present or absent in strains with differential antibiotic production, offering information on strain-specific gene retention or loss potentially associated with adaptive evolution (Figure 4.9).

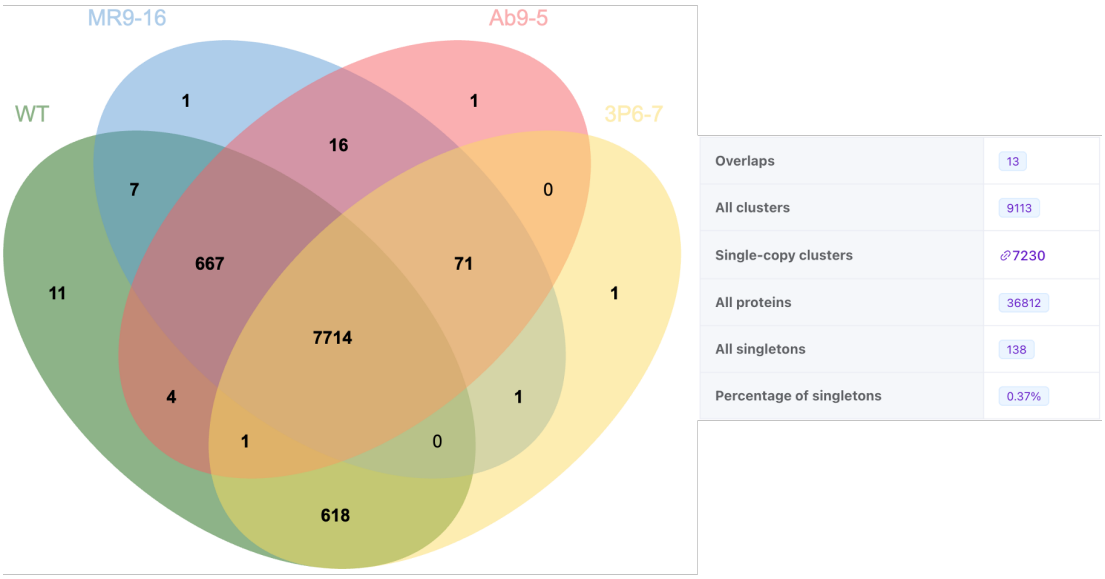

Figure 4.9 Venn diagram of comparative homologous protein clustering and result statics of SSUT88A^{WT} (WT), SSUT88A^{MR9-16} (MR9-16), SSUT88A^{Ab9-5} (Ab9-5), and SSUT88A^{3P6-7} (3P6-7). Generated by Orthovenn3.

Of particular interest, 16 clusters were uniquely shared between the two high antibiotic-producing strains (SSUT88A^{MR9-16} and SSUT88A^{Ab9-5}). Among these were genes associated with RNA secondary structure unwinding and trehalose catabolic processes, while the remainder lacked functional annotations. In contrast, 667 clusters were shared among all three antibiotic-producing strains (wild-type, SSUT88A^{MR9-16} and SSUT88A^{Ab9-5}), representing conserved functions potentially include some those are necessary for bioactivity.

The wild-type shared 618 clusters exclusively with the non-producer strain SSUT88A^{3P6-7}, which may represent gene content that is unnecessary for the enhanced antimicrobial activity. One unique cluster was identified in each of the evolved strains, though none showed known annotated functions.

The wild-type also contained 11 unique clusters, but only one (a transmembrane transporter) had an identifiable function. Additionally, 71 clusters were found to be shared among all evolved strains but absent in WT, which could be derived from co-culture pressure. These two groups were deprioritized as potential natural mutation or background genomic variation independently on selective pressure.

Figure 4.10 demonstrates a phylogenetic tree constructed from the orthologous clusters showed that WT diverged earliest, with SSUT88A^{3P6-7} forming a separate branch prior to the clustering of SSUT88A^{MR9-16} and SSUT88A^{Ab9-5}. While branch lengths were very minimal the topology supports the idea that SSUT88A^{MR9-16} and SSUT88A^{Ab9-5} followed a more similar adaptive path, potentially linked to their enhanced antimicrobial activity.

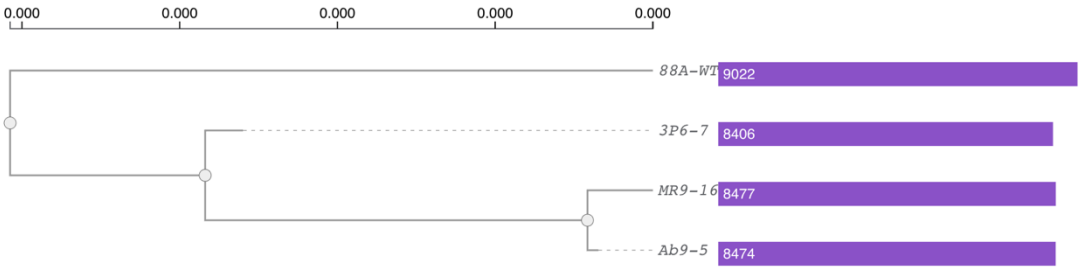

Figure 4.10 Phylogenetic tree based on OrthoVenn-derived orthologous clusters among strains using maximum likelihood method.

While OrthoVenn operates at the amino acid level and clusters genes based on amino acid annotated, antiSMASH provides genes-based predictions specifically for secondary metabolism. Integrating output from both tools allows for a more comprehensive understanding of how gene content and biosynthetic potential have shifted across strains. Therefore, key BGCs identified by antiSMASH were cross-referenced with OrthoVenn clusters to explore whether changes in orthologous content may relate to the observed phenotypic differences. Only the core biosynthetic genes, responsible for the main enzymatic steps in secondary metabolite biosynthesis, of each predicted region were selected for correlation. Due to the complexity and volume of data, representative examples are presented from each comparison group, including cases of both complete and partial correlations. Additional clusters are provided in Appendix B.

For the group of BGCs shared among all antibiotic-producing strains, two representative clusters were examined:

- Mycemycin-like BGC: This complex region includes four core biosynthetic genes. In OrthoVenn, three of these cores formed shared orthologous clusters present in wild-type, SSUT88A^{MR9-16} and SSUT88A^{Ab9-5}. However, one of the clusters also included a homolog from SSUT88A^{3P6-7}, which antiSMASH did not predict to possess this BGC. In this case, SSUT88A^{3P6-7} contributed only one node to the cluster, whereas the antibiotic-producing strains contributed two nodes each. This pattern suggests partial homology in SSUT88A^{3P6-7} at the amino acid

level, potentially reflecting an incomplete biosynthesis process. This suggests that while one of the core genes may still be present in SSUT88A[3P6-7], the other core genes are missing. As a result, antiSMASH likely dropped this region from a complete biosynthetic gene cluster (Figure 4.11A).

- Nucleoside BGC: This cluster, containing a single core biosynthetic gene, showed complete correlation across all three strains in OrthoVenn, comprising one protein from each strain, reflecting strong conservation at the amino acid level and supporting its shared functionality (Figure 4.11B).

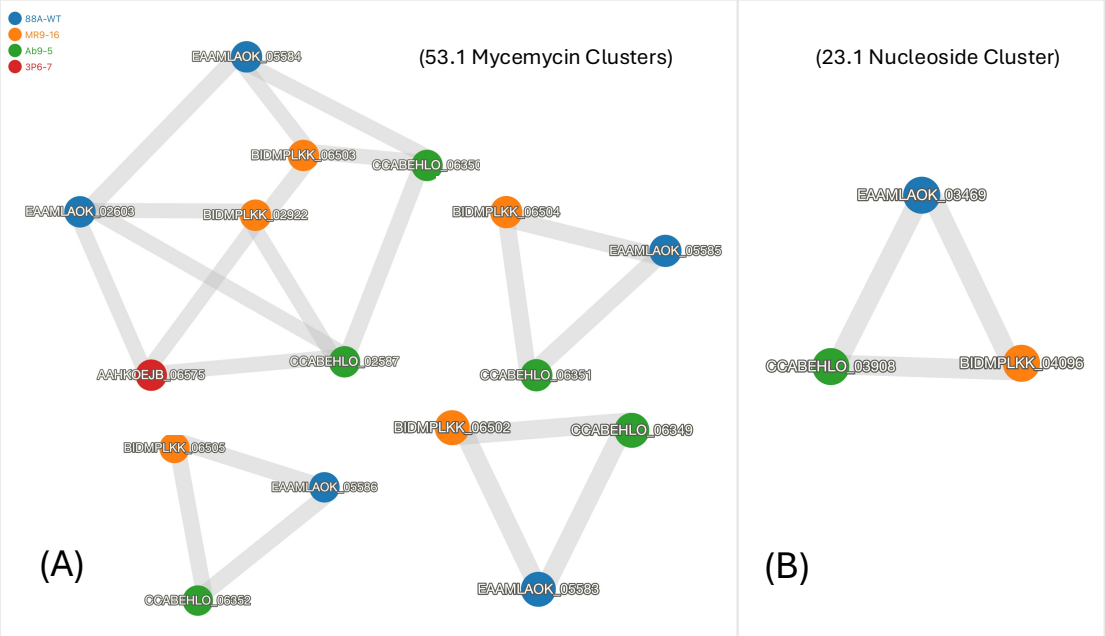

Figure 4.11 Representative OrthoVenn orthologous clustering of core biosynthetic genes from BGCs shared among all antibiotic-producing strains. (A) Mycemycin BGC clusters; (B) Nucleoside cluster.

Among the biosynthetic gene clusters uniquely shared between the two high-antimicrobial-producing strains, the actinomycin D cluster was selected as a representative example (Figure 4.12). Notably, this cluster was identified by antiSMASH with low similarity confidence to known BGCs (see Section 4.5.3). The cluster includes one core biosynthetic gene, which was successfully traced back to its orthologous cluster in OrthoVenn. This correlation supports the functional relevance of this cluster in the enhanced antimicrobial phenotype.

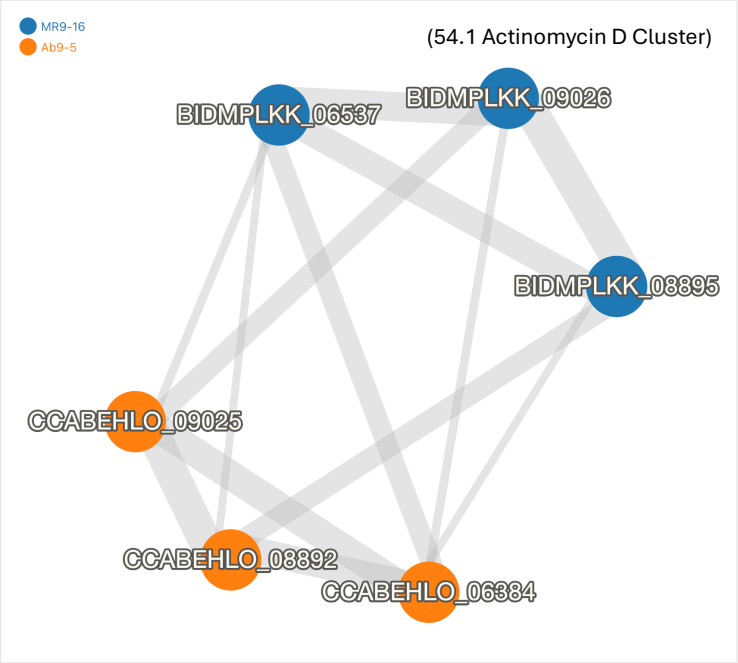

Figure 4.12 Orthologous cluster visualization of core actinomycin D-like biosynthetic genes uniquely shared between high-antimicrobial-producing strains.

Among the biosynthetic clusters shared exclusively between the wild-type the strain lacking antimicrobial activity (SSUT88A^{3P6-7}), two representative clusters were examined: the EDHA-like cluster and a redox cofactor biosynthesis cluster.

- The redox cofactor–associated cluster presented a complex pattern. It contained four core biosynthetic genes, of which three could be correlated in OrthoVenn. Interestingly, the other one orthologous cluster included three nodes from SSUT88A^{3P6-7} and two nodes each from the antibiotic-producing strains. This suggests that some

homologous genes remain in the bioactive strains, but this strain may retain additional or diverged copies. It is possible that this redundancy reflects supplementary functions not directly related to antimicrobial biosynthesis (Figure 4.13A).

- The EDHA cluster, predicted by antiSMASH to encode an aminopolycarboxylic acid-type compound, contained three core biosynthetic genes. All three were found within the same orthologous cluster in OrthoVenn and were exclusive to wild-type and SSUT88A$^{3P6\text{-}7}$ (Figure 4.13B). This strong correlation suggests that these genes are well-conserved at the amino acid level between the two strains, but absent from the evolved bioactive strains. Given that EDHA compounds are not clearly linked to antimicrobial activity, their presence may reflect functions unrelated to the enhanced bioactivity phenotype.

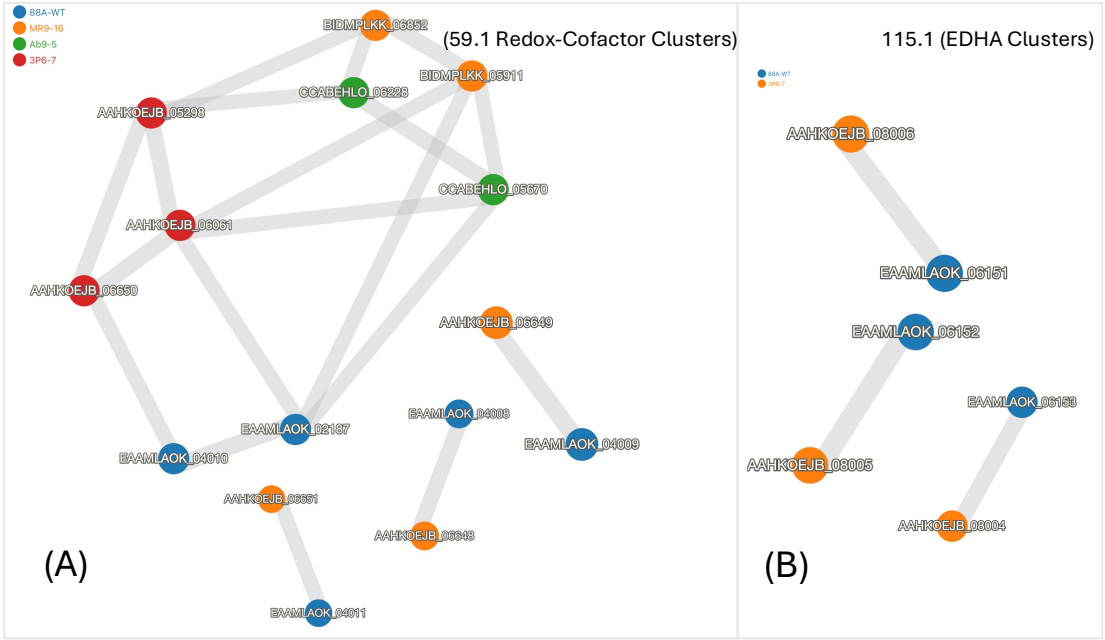

Figure 4.13 Orthologous cluster visualization of biosynthetic gene clusters shared between wild-type and non-producing strain (SSUT88A$^{3P6\text{-}7}$). (A) Redox-cofactor clusters and (B) EDHA cluster.

Taken together, the comparative analysis between antiSMASH-predicted core biosynthetic genes and OrthoVenn orthologous clusters highlights that most core biosynthetic genes identified by antiSMASH could be reliably traced to corresponding orthologous clusters, affirming that functional biosynthetic capacity often aligns with conserved amino acid sequences. However, in some cases, partial clustering or unique node distributions revealed limitations in genome context–based prediction tools.

4.5.5 Structural and Point Mutational Analysis of Adapted Strains

To investigate the genetic basis of phenotypic changes observed in the adapted *Streptomyces* strains, whole-genome resequencing data were analyzed using Breseq, a tool designed to identify mutations relative to a reference genome. Two complementary Breseq modes were used: reference mode (-r) to identify large-scale structural variations, including deletions, duplications, by mapping raw reads against the wild-type reference assembly. And consensus mode (-c) was used to detect small-scale mutations such as single nucleotide polymorphisms (SNPs), short insertions/deletions (indels), and potential frameshift-causing events.

Breseq's reference mode (-r) was used to explore structural changes in the evolved strains by aligning short reads from each evolved genome to the fragmented wild-type draft assembly as an assumed complete reference. The results initially flagged 154 contigs as deleted across at least one evolved genome. However, due to the fragmented nature of the wild-type assembly and the potential for mapping artifacts, these candidates were subjected to additional filtering and validation.

In order to select putative high-possibility true deletions, a multi-step pipeline was employed. First, we re-mapped raw sequencing reads using both Breseq and BWA to ensure consistency across alignment tools. Second, a 31-mer presence/absence analysis using Jellyfish was conducted, querying unique 31-mers from wild-type contigs against the evolved strains' k-mer libraries generated by raw reads. Contigs that showed zero read alignment in both Breseq and BWA, as well as no 31-mer presence, were considered high-confidence deletions. We further visualized

candidate regions using IGV to confirm clean coverage gaps across the contigs. Only deletions supported by all three methods were retained for downstream analysis.

Out of 154 Breseq-flagged deletions, only nine were classified as biologically irrelevant, indicating that the majority of the deletions have high possibility to be true biological events potentially structural genome reduction.

Due to the volume of flagged deletions, every contig analysis was impractical. Instead, representative contigs were selected based on biological relevance, mapping clarity, the curation criteria were demonstrated in Appendix C (Figure S2 – S5).

While the primary interest was in deletions directly impacting secondary metabolism, a subset of biologically relevant deletions that did not directly affect BGCs was also analyzed. These were chosen not as random contrasts, but as informative examples that illustrate the broader view of genome reduction during adaptation.

The goal was to highlight that although not all deletions can be confidently said that they were tied to antimicrobial production, many still reflected meaningful structural or regulatory changes. We grouped the selected deletions into two categories:

(A) Deletions not contributing to BGCs were selected based on high relative read depth in the wild-type and retained genome, with the absence across mapping/31-mer validation. To ensure the selected cases were biologically informative, we chose representatives that exemplified the range of observed deletion patterns including:

- Contig 112, which was deleted in high-activity stains SSUT88A^{MR9-16} and SSUT88A^{Ab9-5} with no detected MGE (Figure 4.14). Breseq and BWA mapping show complete loss of read alignment in the evolved strains relative to SSUT88A^{3P6-7}. k-mer analysis confirms absence of contig-specific 31-mers. Annotations reveal no MGEs, suggesting a dispensable region was purged during adaptive evolution.

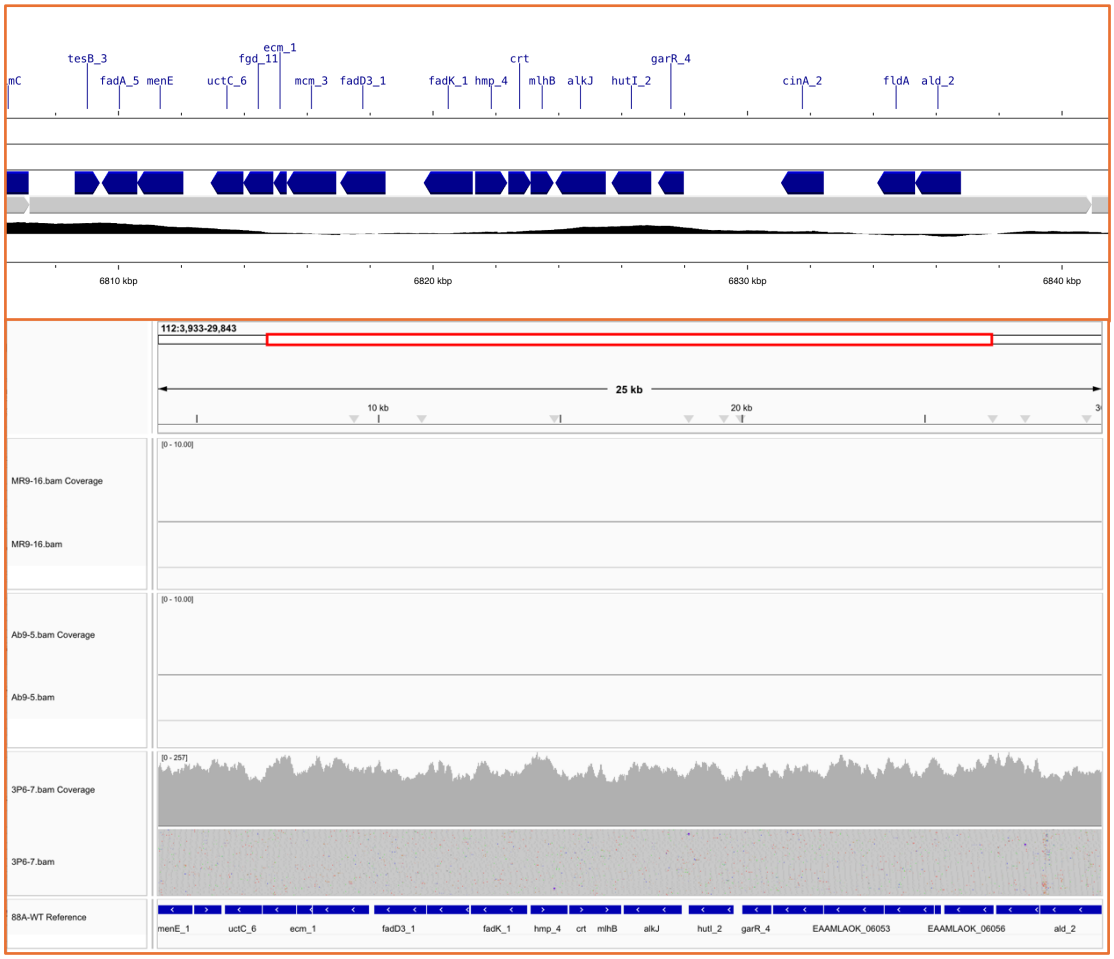

Figure 4.14 Deletion of contig 112 in SSUT88A^{MR9-16} and SSUT88A^{Ab9-5} without MGE signatures.

- Contig 108, which was deleted in the stains SSUT88A^{MR9-16} and SSUT88A^{Ab9-5}. This contig encoded *OppF*, a transporter typically associated with MGE contexts, potentially related to mechanisms during laboratory adaptation evolution. Read mapping and k-mer absence validate loss of the contig in both high-activity strains. Annotation identifies *oppF*, a component of an oligopeptide permease system often found in mobile or horizontally transferred regions (Figure 4.15).

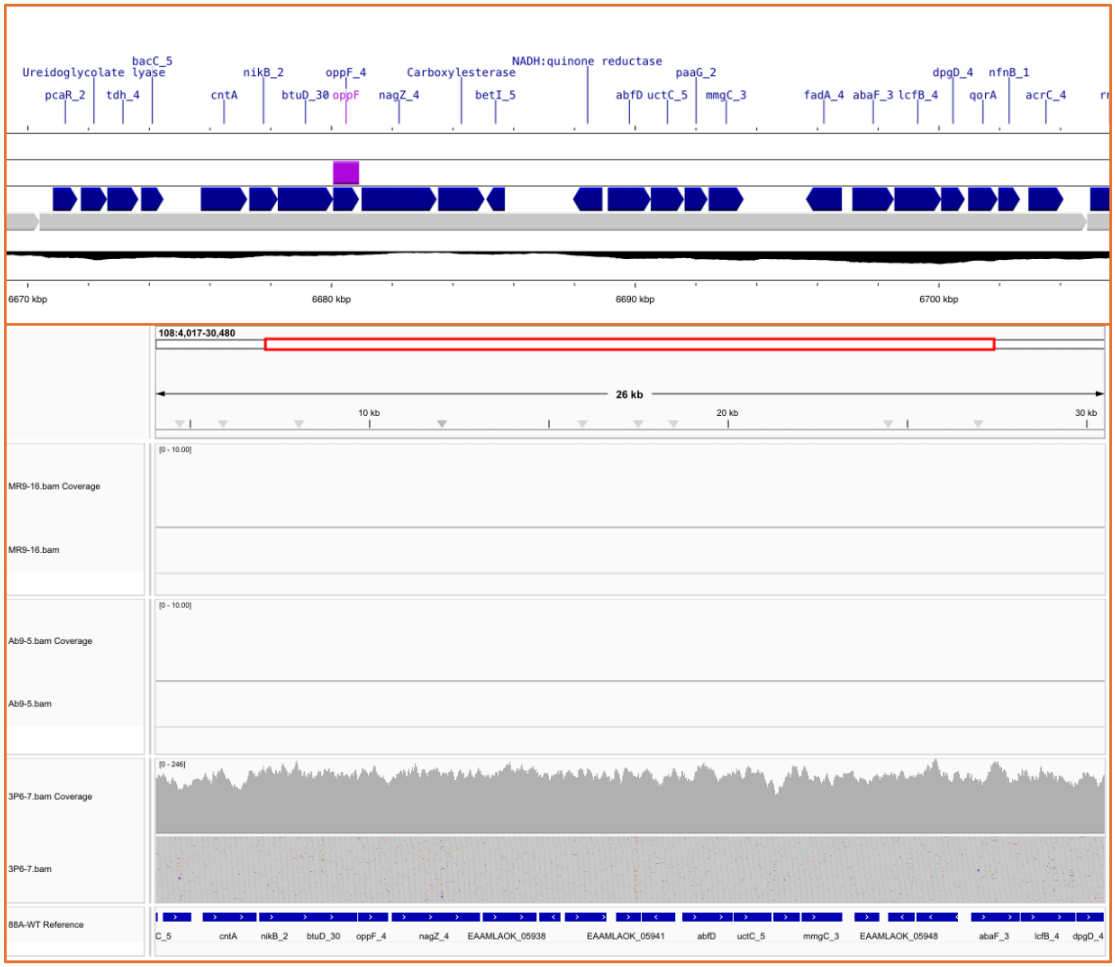

Figure 4.15 Deletion of contig 108 in SSUT88A^{MR9-16} and SSUT88A^{Ab9-5} with putative MGE-associated transporter gene *oppF*.

- Contig 141, a SSUT88A^{3P6-7} deleted contig without MGE annotated (Figure 4.16). Absence of read coverage and k-mer matches confirm a SSUT88A^{3P6-7}-specific deletion. Functional annotation shows no MGE-related domains, consistent with a non-mobile but nonessential region being deleted in the low-activity strain.

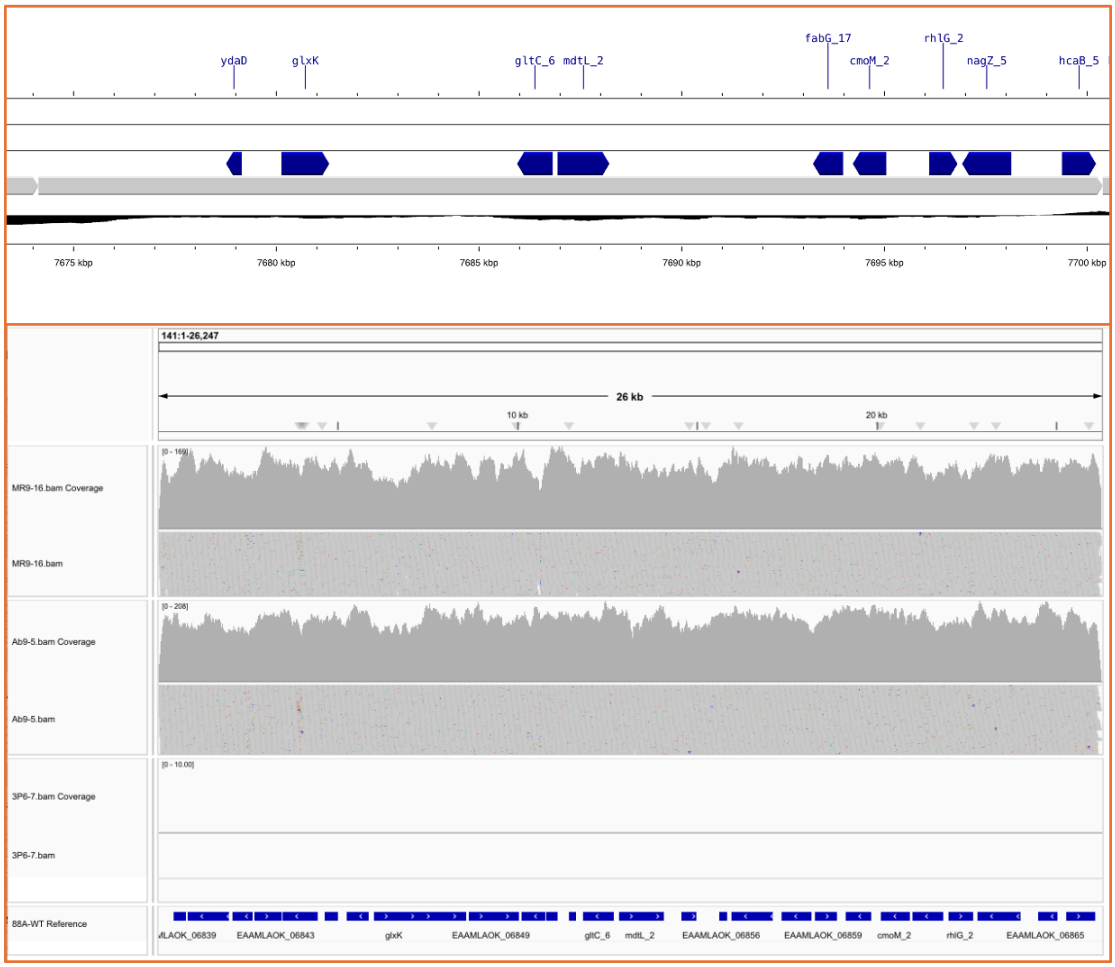

Figure 4.16 Loss of contig 141 in SSUT88A^{3P6-7}, with no detected mobile genetic elements.

- Contig 136, loss contig from non-activity producing strain SSUT88A^{3P6-7} with five integration/excision MGEs. The absence in the strain across all validation criteria. Annotation reveals five genes associated with integration and excision functions, including transposases (*tpase*) and hypothetical integrases (R00164). This could indicate that mobile genetic elements contributed to genome instability and were selectively removed (Figure 4.17).

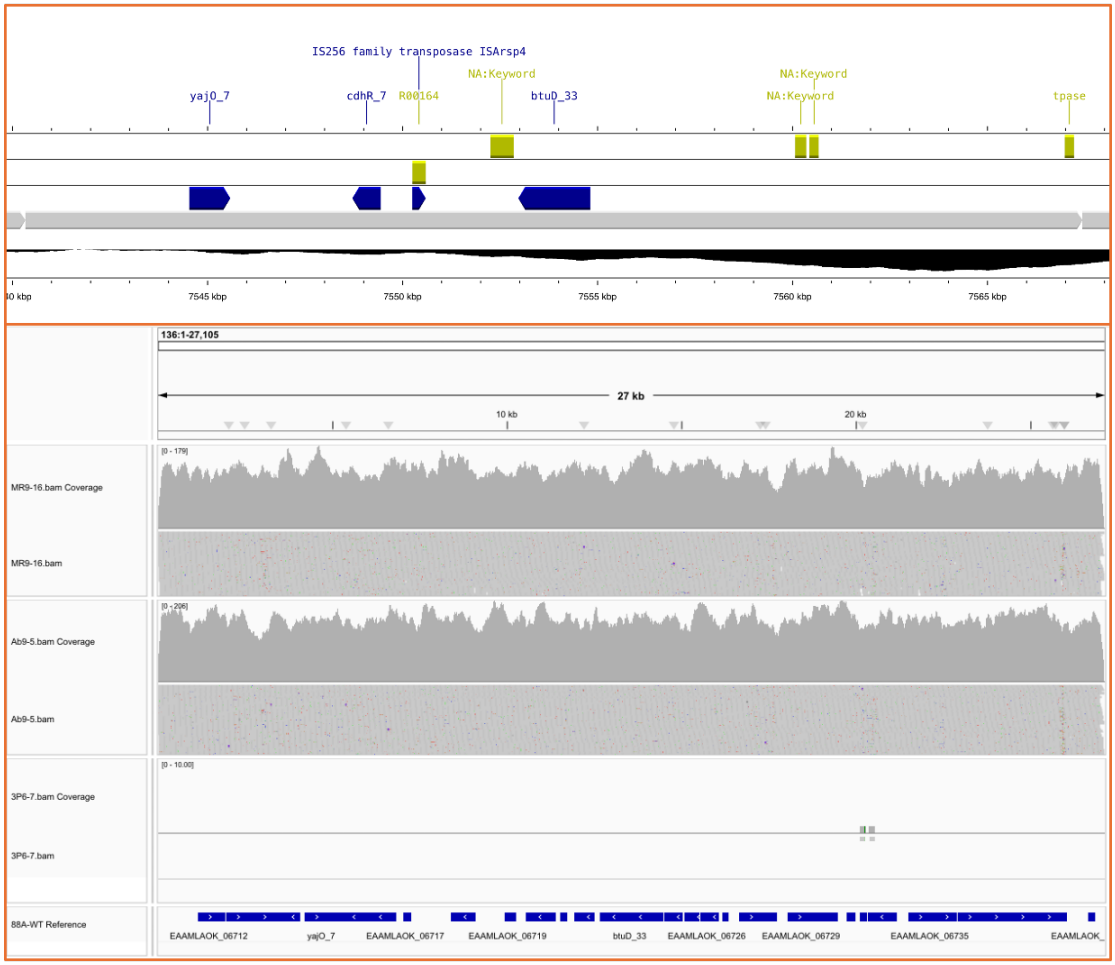

Figure 4.17 Loss of contig 136 in SSUT88A^{3P6-7}, containing multiple mobile element-related genes.

(B) Deletions Correlated with Secondary Metabolism and Ortholog Clusters contributing to BGCs

- Contig 48 (lost in SSUT88A^{3P6-7}) corresponded to a nucleoside cluster found in wild-type, SSUT88A^{MR9-16} and SSUT88A^{Ab9-5} by both OrthoVenn and antiSMASH, but absent in SSUT88A^{3P6-7}. No MGE signatures were found, supporting selective deletion (Figure 4.18). Based on both OrthoVenn and antiSMASH predictions. Its deletion was confirmed by mapping and k-mer analysis. No MGE domains were identified, suggesting this was a stable but metabolically costly region lost under disadvantageous selective pressure.

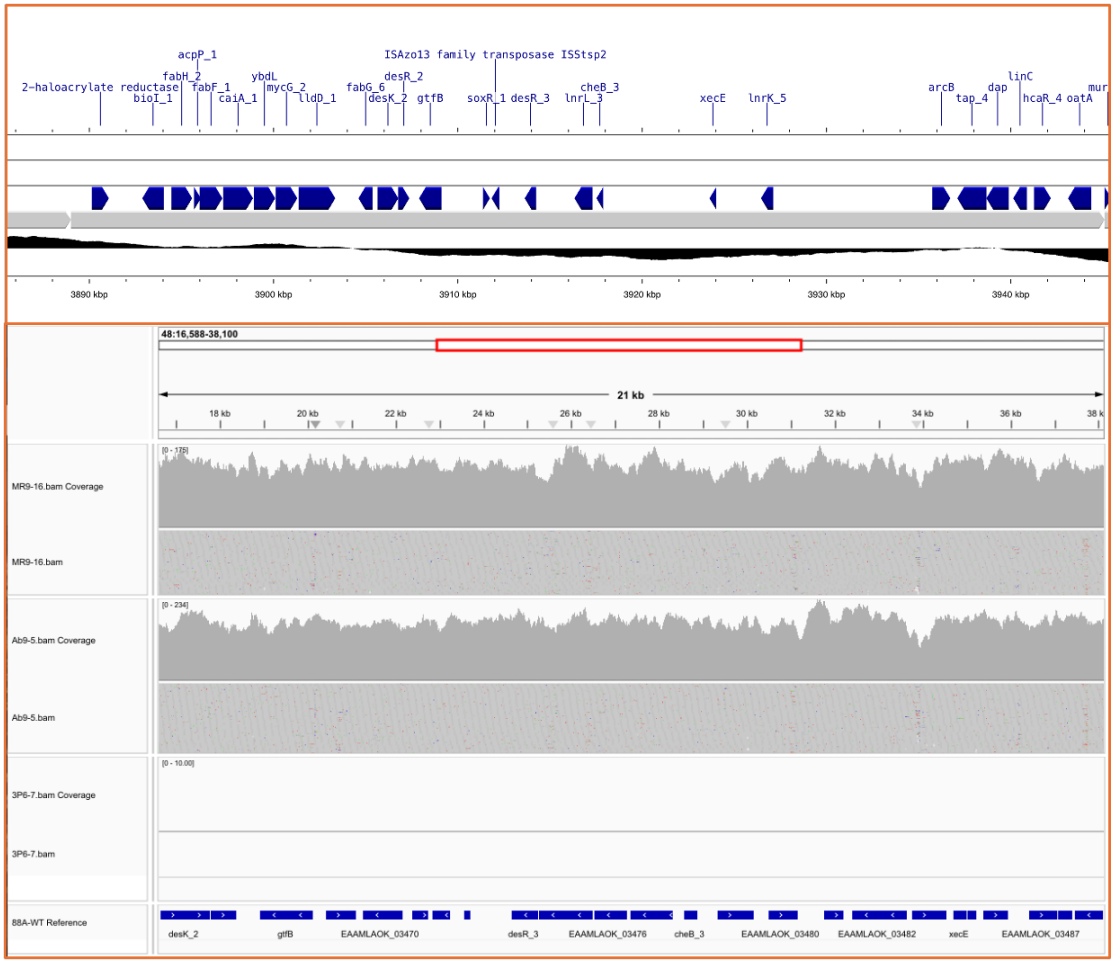

Figure 4.18 Deletion of contig 48 in SSUT88A^{3P6-7} associated with a nucleoside biosynthetic cluster.

- Contig 97 (also lost in SSUT88A^{3P6-7}) encoded the Mycemycin BGC, flagged by antiSMASH and linked to multiple ortholog clusters. One integration/excision-associated MGE was annotated, but the broader cluster loss suggests functional deletion (Figure 4.19). The contig was fully deleted in SSUT88A^{3P6-7}. Annotation detected one integration/excision-associated gene of unknown annotation.

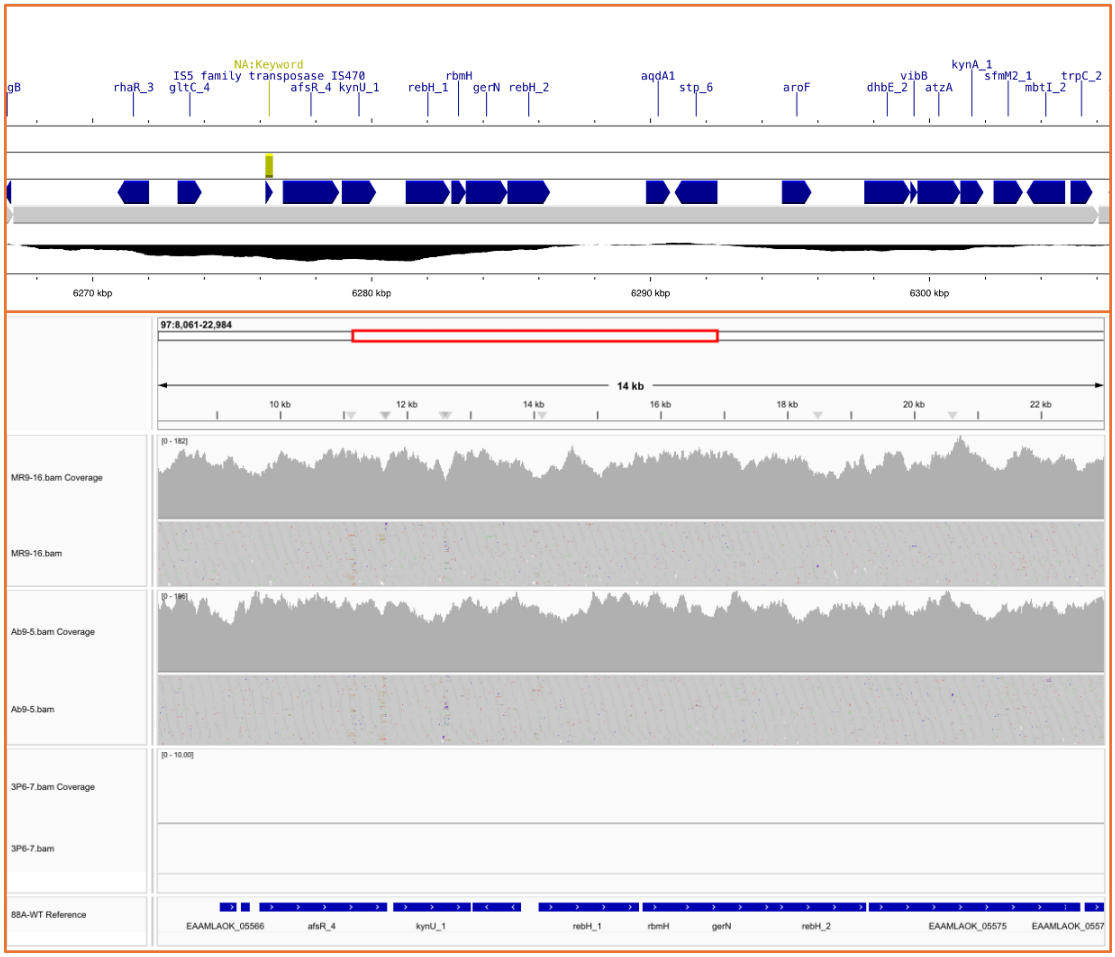

Figure 4.19 Loss of contig 97 in SSUT88A^{3P6-7}, encoding the Mycemycin BGC with partial MGE involvement.

- Contig 59 (lost in SSUT88A$^{MR9\text{-}16}$ and SSUT88A$^{Ab9\text{-}5}$) was linked was linked to multiple OrthoVenn clusters and biosynthetic genes predicted to contribute to redox cofactor pathways. Its complete deletion, without MGE signatures (Figure 4.20), supports the notion of functional gene loss driven by adaptive metabolic evolution.

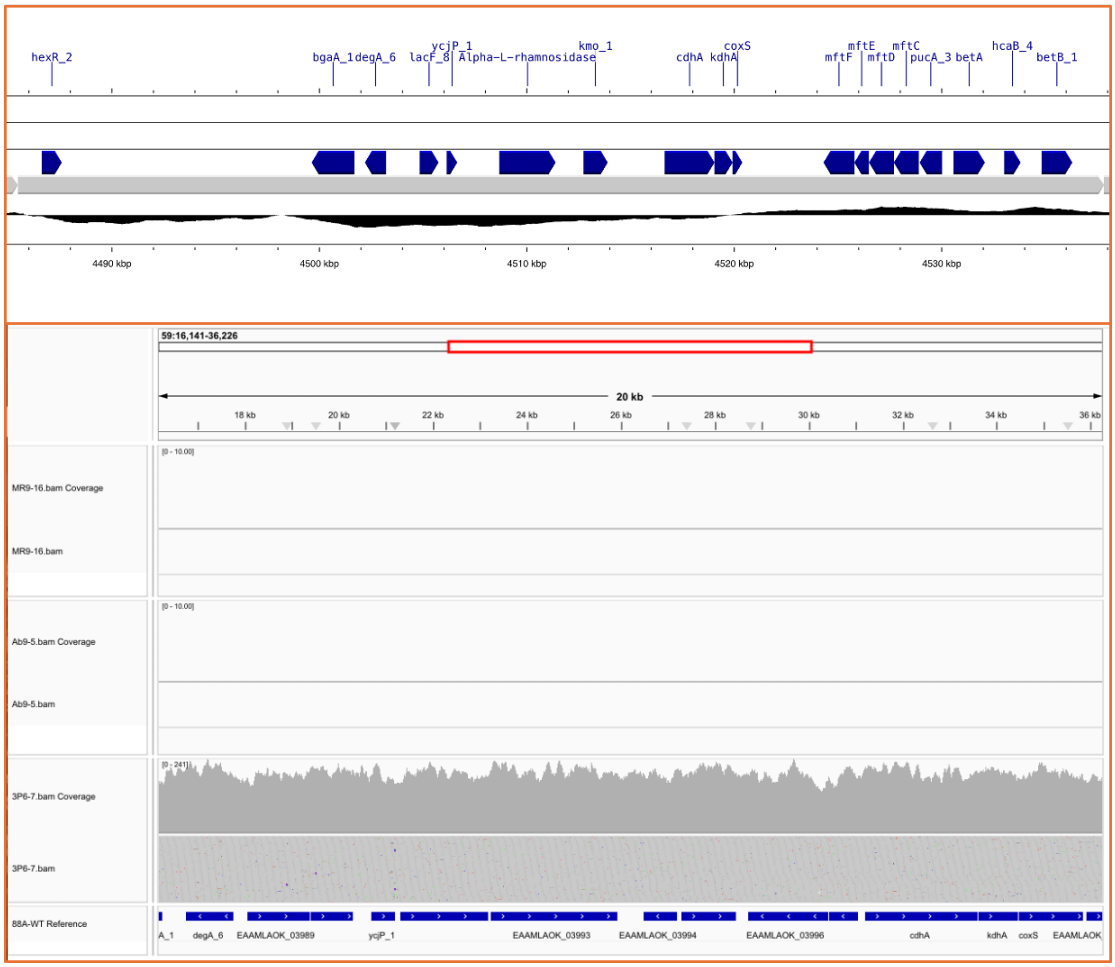

Figure 4.20 Deletion of contig 59 in SSUT88A$^{MR9\text{-}16}$ and SSUT88A$^{Ab9\text{-}5}$associated with redox cofactor biosynthesis.

- Contig 115 (also lost in SSUT88A^{MR9-16} and SSUT88A^{Ab9-5}) encoded genes related to EDHA biosynthesis, overlapping with four ortholog clusters, but showed no MGE domains (Figure 4.21). This contig overlaps with four OrthoVenn clusters and harbors EDHA-related genes, as identified in antiSMASH outputs. Despite its biosynthetic relevance, no mobile genetic elements were detected, indicating that deletion was not mediated by MGEs.

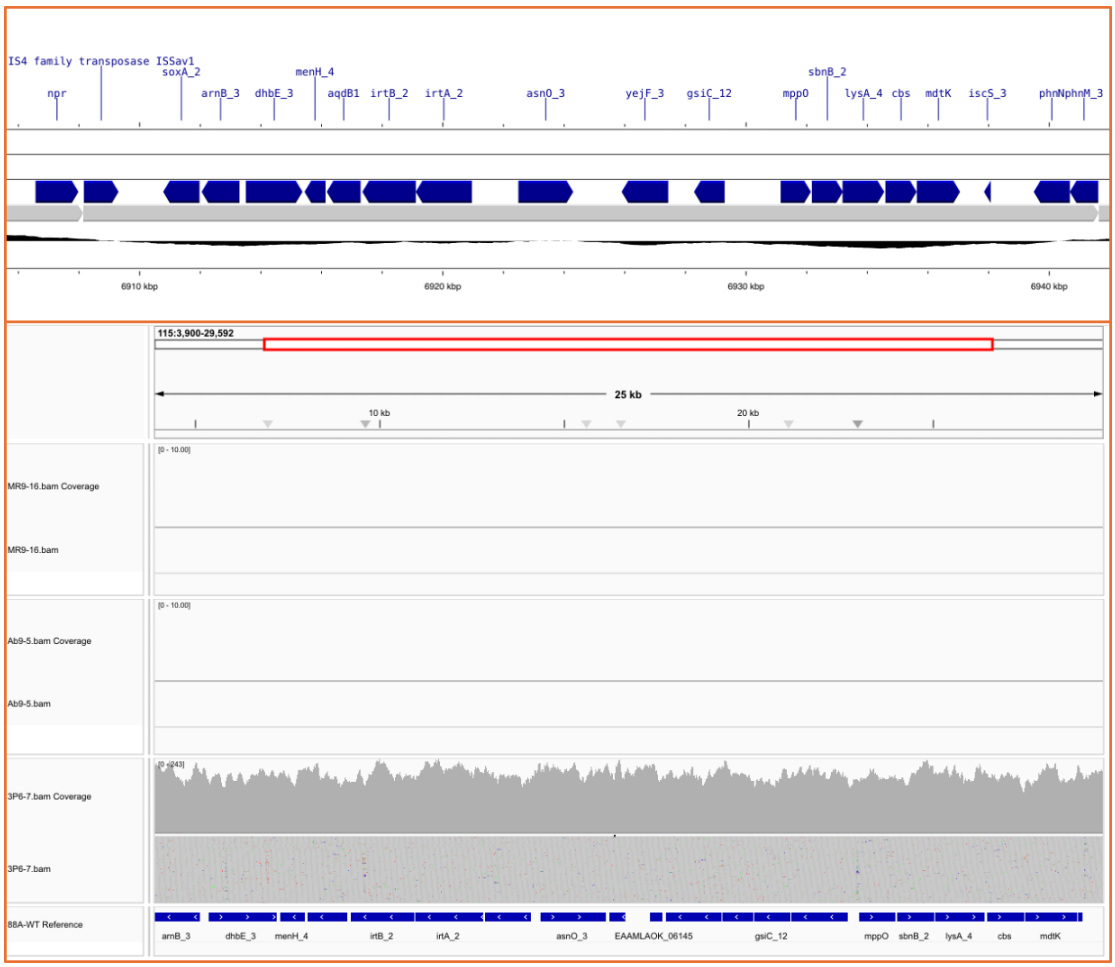

Figure 4.21 Loss of contig 115 in SSUT88A^{MR9-16} and SSUT88A^{Ab9-5}, associated with EDHA biosynthesis.

While we cannot rule out all technical sources of contig absence, we believe that some deletions observed in this study could be true biological losses. Illumina sequencing libraries were prepared using random fragmentation, ensuring

broad genomic coverage (CD-Genomics, 2025). If random dropout or assembly gaps were responsible, we would expect inconsistent patterns across strains or partial mapping within contigs. Instead, we observed clean, strain-specific deletions, which were highly biologically correlated. These were independently confirmed with Breseq, BWA, k-mer analysis, and IGV visualization. Moreover, only 9 out of 154 Breseq-flagged deletions failed to meet our validation criteria, suggesting that the majority were not due to technical noise.

To identify small-scale genomic variants potentially responsible for adaptive phenotypes in evolved strains, the short-read data from SSUT88A$^{MR9\text{-}16}$, SSUT88A$^{Ab9\text{-}5}$, and SSUT88A$^{3P6\text{-}7}$ were analyzed using Breseq v0.38.1 in consensus mode (-c). This method does not rely on alignment to a fragmented reference genome but instead reconstructs each sample as an independent contig. It enables the detection of point mutations, particularly SNPs, with reduced susceptibility to reference-related artifacts. Consensus mode was used in addition to reference mode for its improved sensitivity of small-scale detections.

The Initial outputs yielded a large number of candidate SNPs across the evolved strains. However, a stringent manual curation workflow was applied to refine the dataset. Candidate mutations were assessed for sequencing depth, mutation quality scores, alignment confidence in surrounding bases, and potential biological relevance. Through this conservative filtering, only three high-confidence SNPs were retained.

- Shared SNP in High-Antibiotic-Producing Strains (SSUT88A$^{MR9\text{-}16}$ and SSUT88A$^{Ab9\text{-}5}$): A single nucleotide polymorphism was identified in the intergenic region between *valS* (valyl-tRNA synthetase) and *murE_2* (UDP-N-acetylmuramoylalanine–D-glutamate ligase), located 37 base pairs upstream of *murE_2*. While the exact promoter boundaries are unconfirmed, this position falls near where a -35 motif of a **σ**^70 promoter would be expected, raising the possibility of regulatory impact. *murE_2* is involved in peptidoglycan biosynthesis via the addition of diamino acid (*meso*-diamino-pimelate or *L*-lysine) to UDP-N-acetylmuramoyl-L-alanyl-D-glutamate (UMAG) (Mol et al., 2003), and

the mutation's consistent presence in both high-producing strains suggests it may contribute to peptidoglycan alteration or adaptive evolution under co-culture selective stress, though further functional validation would be needed (Figure 4.22).

- Unique SNP in the SSUT88A$^{Ab9\text{-}5}$ (Precocious Antibiotic-Producing Strain): This mutation lies in the intergenic region between EAAMLAOK_05902 and EAAMLAOK_05903 (Prokka annotation ID), positioned 14 base pairs upstream of EAAMLAOK_05903. While both genes were annotated as hypothetical proteins, BLASTP analysis revealed that EAAMLAOK_05903 encodes a conserved protein with a DUF2637 (*SpdA*-like) domain, widely distributed in *Streptomyces* species. Although its exact function is unclear, the SNP's proximity to the presumed promoter region, potentially within striking distance of a -10 motif of **σ** factor, makes a regulatory role plausible, therefore speculative. This mutation could fine-tune expression of a yet-uncharacterized regulator, possibly contributing to the early or enhanced secondary metabolism observed in this strain (Figure 4.23).
- Unique SNP in the Pigment-Deficient, Activity-Loss Strain (SSUT88A$^{3P6\text{-}7}$): A silent coding mutation was detected within a gene annotated as Prokka-Annotated hypothetical protein ID, EAAMLAOK_05879, where the codon CGG (arginine) was changed to AGG (another synonymous arginine codon). Notably, this mutation occurs at the first base of the codon, meaning it is not a case of typical third-base redundancy, which is observed more frequently. While the protein sequence remains unchanged, studies have found that synonymous mutations can still influence biological function through various effects on mRNA secondary structure, translational efficiency, or codon usage bias (Plotkin and Kudla, 2011). In addition, consequences of synonymous mutations' functionality and non-neutrality for numerous analyses and conclusions relevant to genetics, evolution, conservation, and illness, have been proposed (Zhang and Qian, 2025). Some studies even stated

that “synonymous mutations in representative yeast genes are mostly strongly non-neutral” (Shen et al., 2022). Given its exclusive presence in the SSUT88A$^{3P6\text{-}7}$ strain, which exhibits both pigment loss and diminished antimicrobial activity, this mutation may subtly disrupt regulatory dynamics at the RNA level or interfere with precise protein expression control (Figure 4.24).

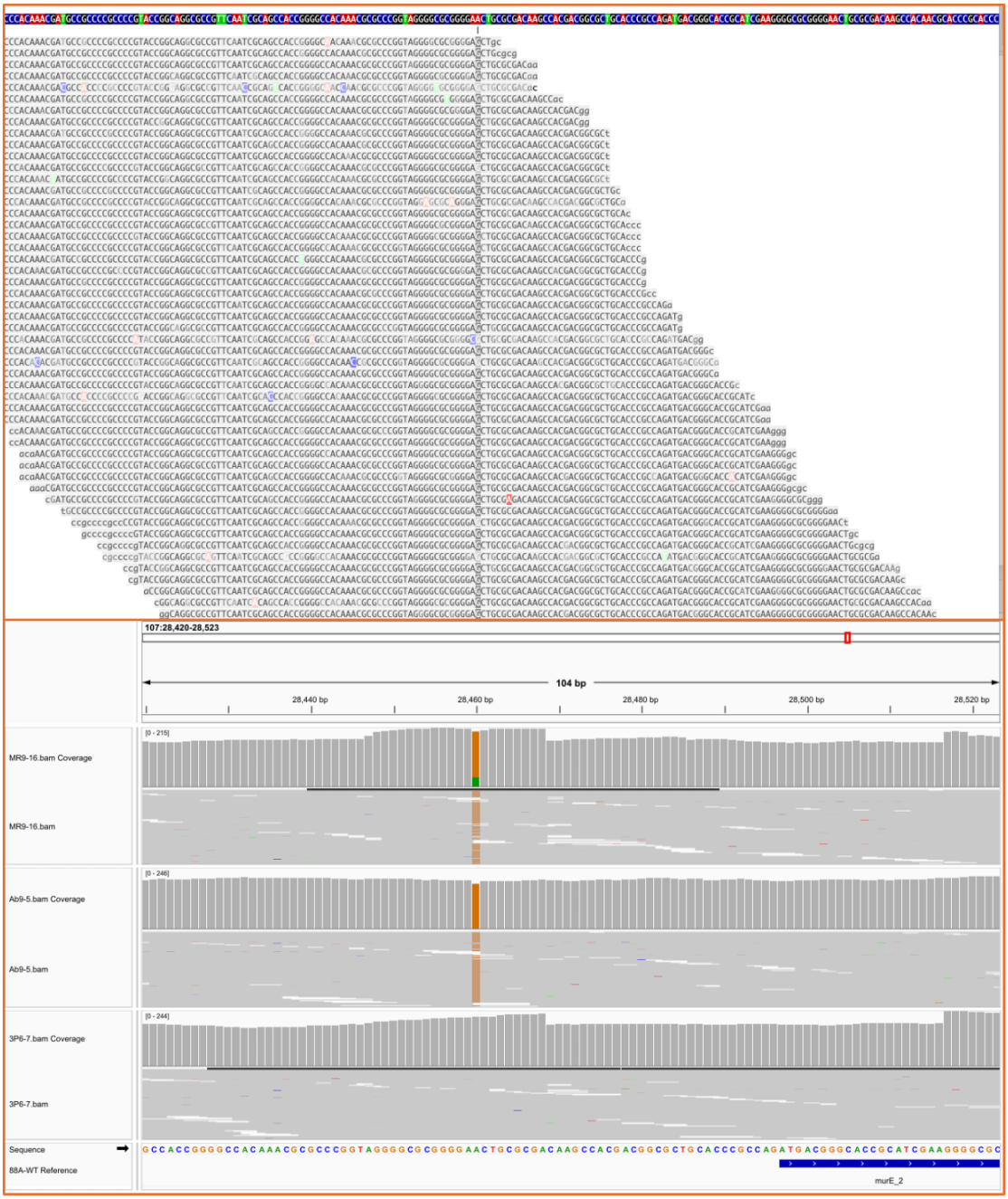

Figure 4.22 Shared SNP in High-Antibiotic-Producing Strains.

Breseq and IGV visualizations of a shared intergenic SNP located –37 bp upstream of *murE_2* (UDP-N-acetylmuramoylalanine–D-glutamate ligase), between *valS* and *murE_2*. The mutation is present in both SSUT88A$^{MR9\text{-}16}$ and SSUT88A$^{Ab9\text{-}5}$, but absent in the wild-type and SSUT88A$^{3P6\text{-}7}$. The mutation site is proximal to the theoretical -35 promoter region of *murE_2*, potentially impacting transcriptional regulation and contributing to enhanced antibiotic production.

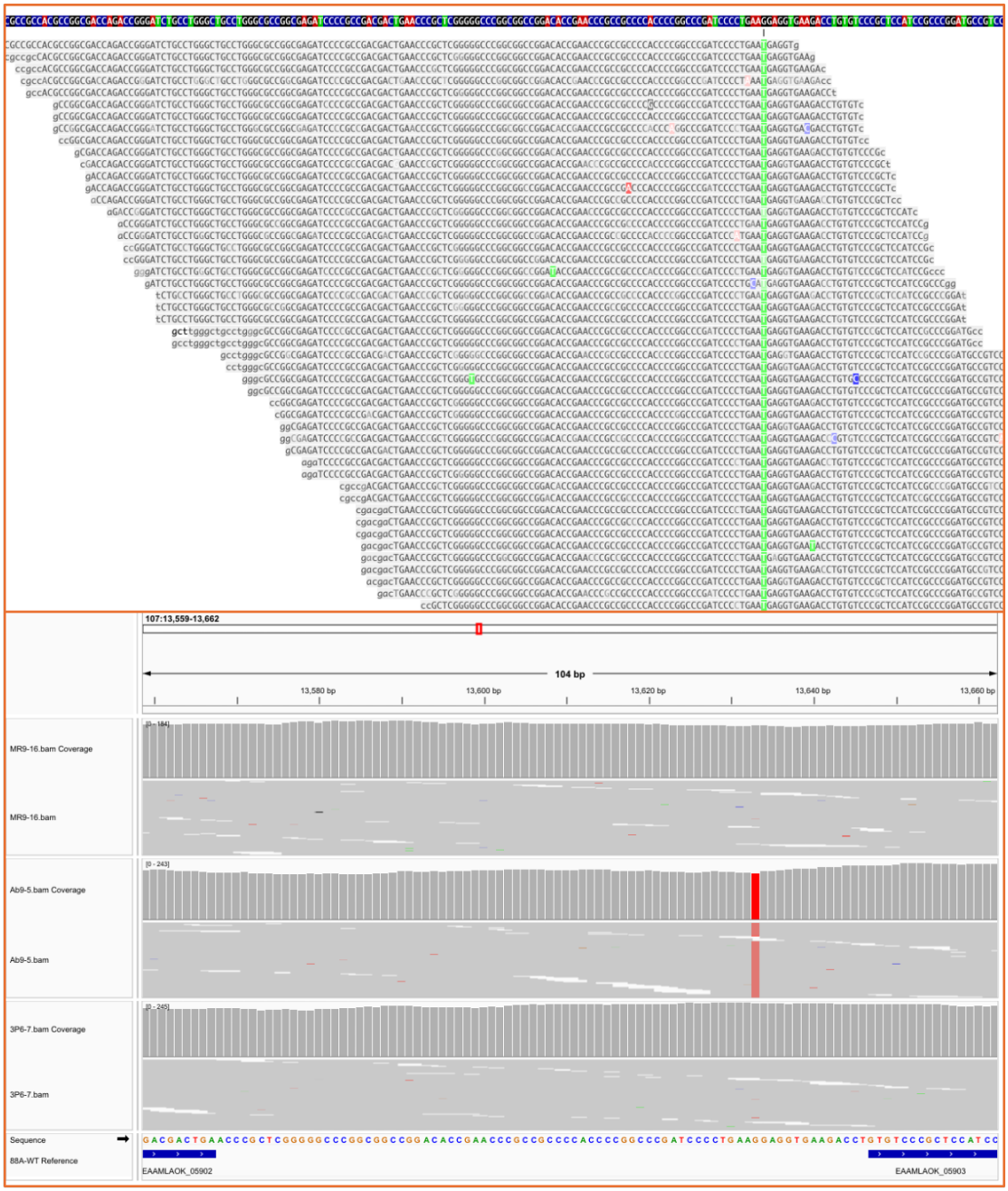

Figure 4.23 Unique SNP in the SSUT88A$^{Ab9\text{-}5}$ (Precocious Antibiotic-Producing Strain). Breseq and IGV snapshots highlighting a unique intergenic SNP in SSUT88A$^{Ab9\text{-}5}$, located −14 bp upstream of EAAMLAOK_05903. The mutation is absent in other strains. Its location is immediately upstream of a gene later identified (via BLASTP) as encoding a DUF2637 (*SpdA*-like) domain-containing protein. The mutation lies close to the presumed -10 region of the promoter, potentially influencing early or enhanced antibiotic production via regulatory alteration.

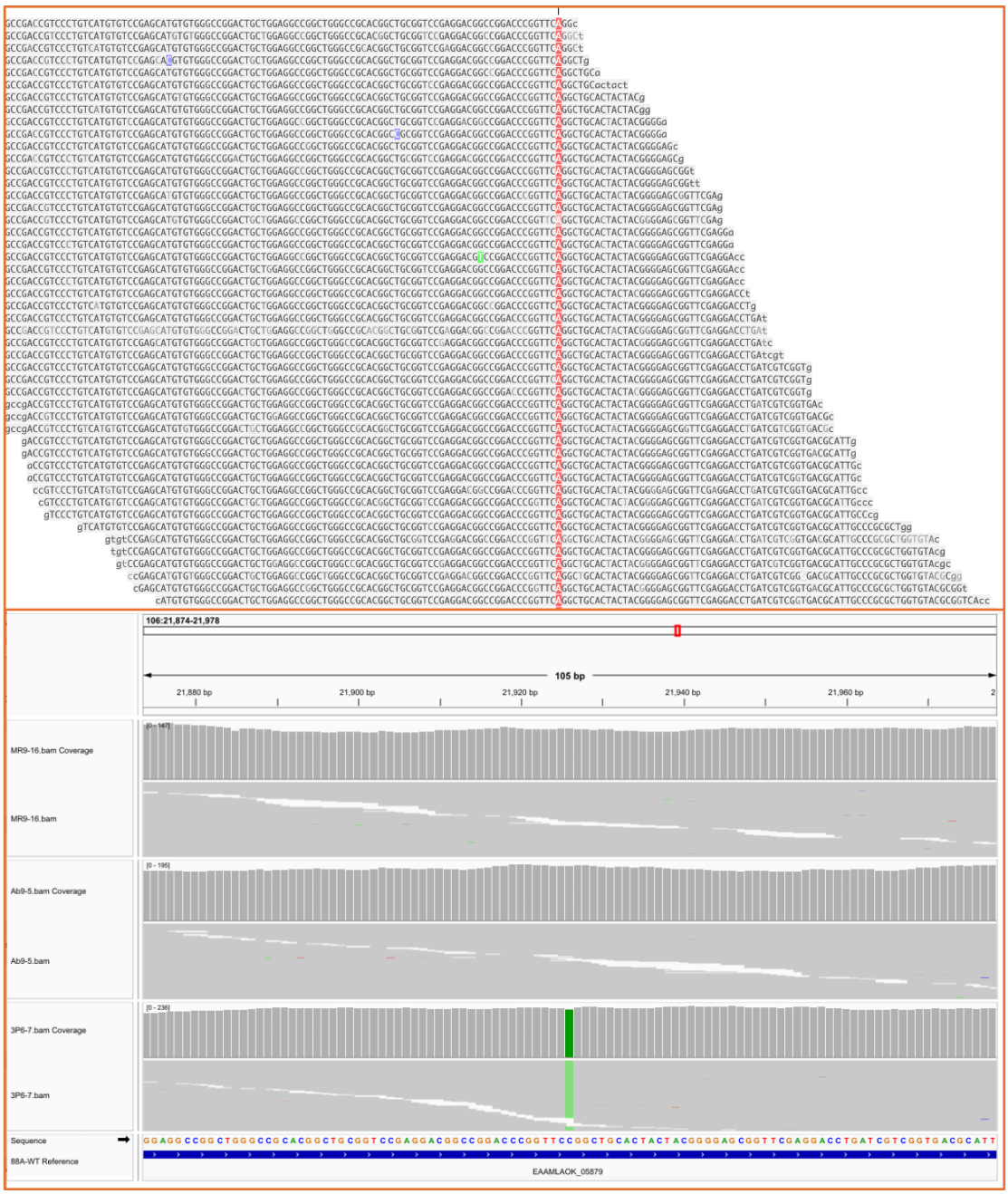

Figure 4.24 Unique SNP in the Pigment-Deficient, Activity-Loss Strain (SSUT88A$^{3P6\text{-}7}$). Breseq and IGV views of a unique silent mutation (CGG ⟶ AGG; Arg⟶Arg) found exclusively in SSUT88A$^{3P6\text{-}7}$ within EAAMLAOK_05879, a gene annotated as a hypothetical protein. Though the protein sequence remains unchanged, possible functional effects include altered mRNA structure, codon usage bias, or translational efficiency, which may relate to the observed loss of pigmentation and antimicrobial activity.

Together, the Breseq -r and -c mode analyses provided complementary insights into the genomic basis of phenotypic divergence among evolved strains. Reference alignment mode (-r) enabled detection of large-scale structural changes such as deletions, many of which were validated by k-mer analysis, MGE annotation, and orthology-based context. These structural changes helped explain varied phenotypic traits through the potential loss of biosynthetic gene clusters. On the other hand, consensus mode (-c) revealed a small set of high-confidence SNPs.

The combined functional genomics approach across antiSMASH, OrthoVenn, and Breseq analyses reveals a complex and layered picture of adaptive evolution in the strains subjected to co-culture pressure. Each method contributed a unique resolution. Together, these analyses show that increased or diminished antimicrobial activity correlates with multiple layers of genomic change. High-producing strains retained and shared a core of biosynthetic clusters and unique orthologs, while simultaneously acquiring targeted deletions and a shared regulatory SNP. Conversely, the loss-of-function SSUT88A$^{3P6\text{-}7}$ strain exhibited deletions of key clusters (e.g., mycemycin), pigment-associated regions, and unique SNPs potentially affecting translation or regulation. Additionally, Mobile genetic elements were unevenly associated with deletions, suggesting that some genomic remodeling occurred via excision-mediated mechanisms, while others may reflect selective pressures acting on non-mobile but functionally important loci.